

HEAT TRANSFER AND FLOW BEHAVIOR OF CARBON BASED NANOFLUIDS

by

Çayan Demirkır

B.S., Mechanical Engineering, İstanbul Technical University, 2016

Submitted to the Institute for Graduate Studies in
Science and Engineering in partial fulfillment of
the requirements for the degree of
Master of Science

Graduate Program in Mechanical Engineering
Boğaziçi University

2019

ACKNOWLEDGEMENTS

First of all, I would like to express my profound gratitude and sincere thanks to my advisor, Prof. Hakan Ertürk for his academic support, motivation and kind patience. He has always contributed to my academic development and scientific vision since the day I visited him as a candidate master student three years ago. Besides, I am also indebted to him for inspiring me to start running.

I would like to thank our faculty members for developing my academic knowledge during master courses I had taken. Also, I would like to thank Boğaziçi University for support under B.U. Research Fund AP-15302.

I could not have completed this study without my family's endless support. They have always believed me, stood by me, and helped me to overcome the difficulties. I feel so lucky to have such a great family and, I would like to thank my mother Halime, my father Hüseyin, and my sister, Ceren.

I would also like to thank each of the TESLAB members for their valuable friendship. At the beginning of my master study, Beybin and Özgür made substantial contributions to the formation of my experimental know-how. Moreover, I feel very pleasant for getting a chance to meet with my dear friends Canberk, Dilan and Refet in here. This study became more enjoyable with their help and precious companionship. Also, I would like to thank my dearest friend, dormitory bunkmate and then, housemate, Hasan due to his support in every part of my life.

Above all, I would like to dedicate this thesis to my dear love İzel. In addition to her wholehearted support and infinite patience in the last couple of years, I am more than grateful to her for changing the way of my life since the day we first met.

ABSTRACT

HEAT TRANSFER AND FLOW BEHAVIOR OF CARBON BASED NANOFLUIDS

Thermal and rheological behaviors of the graphene-water nanofluids are investigated experimentally. Nanofluids with particle mass fraction from 0.025 to 2.0% are prepared by using PVP as surface active material and ultrasonication. Morphological, material and stability characterization are carried out by STEM imaging, Raman spectroscopy, and zeta potential measurements. Rheological behavior of the prepared samples is analyzed at different temperatures and shear rates. Maximum viscosity increase is observed to be 45% for the 2.0% mass concentration at 25°C. The relative viscosity does not change with temperature, unlike the absolute viscosity that decreases with temperature due to the viscosity change of the base fluid. Moreover, the relative viscosity is nearly constant at low concentrations for all shear rates, and it decreases with increasing shear rate for the mass fractions higher than 1.0%. Hence, graphene-water nanofluids exhibit Newtonian behavior for particle mass fractions below 1.0% and shear thinning behavior at higher concentrations. Hysteresis is observed when increasing and reducing the shear rates within the same speed ranges for the samples higher than 1% particle mass fraction and above 40°C. Thermal conductivity is enhanced with increasing concentration and maximum augmentation is observed to be 96% for a mass fraction of 2.0%. Forced convection is investigated for graphene-water nanofluids of 0.025, 0.1 and 0.2% mass fractions at a Reynolds numbers from 1400 to 4000. Transition to turbulence is observed at lower Reynolds numbers for 0.1 and 0.2% concentrations. Maximum heat transfer enhancement is measured as 36% for 0.2% nanofluid for a Reynolds number of 3950. Besides, pressure drop and friction factor measurements are carried out. Maximum pressure loss is observed to increase 30% at transition region.

ÖZET

KARBON TABANLI NANOAKIŞKANLARIN ISI TRANSFERİ VE AKIŞ DAVRANIŞI

Grafen-su nanoakışkanların ısıl ve reolojik davranışları deneysel olarak incelendi. %0.025 ile %2.0 parçacık kütle konsantrasyonuna sahip nanoakışkanlar yüzey aktif madde olarak PVP kullanılarak ve ultrasonik olarak karıştırılarak üretildi. Morfolojik, malzeme ve stabilite karakterizasyonu STEM görüntüleme, Raman spektroskopisi ve zeta potansiyel ölçümleri ile uygulandı. Hazırlanan örneklerin reolojik davranışı farklı sıcaklık ve kesme hızlarında analiz edildi. Maksimum viskozite artışı, %2.0'lık konsantrasyona sahip örnek için 25 °C'de %45 olarak gözlemlendi. Bağlı viskozite, baz akışkandaki viskozite değişiminden dolayı sıcaklıkla azalan mutlak viskozitenin aksine sıcaklık ile değişmemektedir. Ayrıca, bağlı viskozite düşük konsantrasyonlarda tüm kesme hızları için neredeyse sabittir ve %1.0'ın üzerindeki kütle konsantrasyonları için artan kesme hızlarıyla azalır. Bu yüzden grafen-su nanoakışkanları %1.0'ın altındaki parçacık kütle konsantrasyonlarında Newtonyan davranış, daha yüksek konsantrasyonlarda ise kesme incelmesi davranışı sergiler. 40°C ve %1.0 parçacık kütle konsantrasyonu üzerinde kesme hızları aynı hız aralığında arttırıldığında ve azaltıldığında histerezis gözlemlenir. Isıl iletkenlik artan konsantrasyonla artar ve maksimum artış %2 kütle konsantrasyonu için %96 olarak gözlemlenmiştir. Grafen-su nanoakışkanların taşınimsal ısı transferi %0.025, %0.1 ve %0.2 kütle konsantrasyonlarında 1400'ten 4000'e kadar olan Reynolds sayılarında araştırılmıştır. %0.1 ve %0.2 kütle konsantrasyonlarındaki nanoakışkanlar için türbülansa geçişin daha düşük Reynolds sayılarında olduğu gözlemlenmiştir. Maksimum ısı transferi artışı %2'lik nanoakışkan için 3950 Reynolds sayısında %36 olarak ölçülmüştür. Ayrıca, basınç düşüşü ve sürtünme katsayısı için ölçümler yapılmıştır. Maksimum basınç düşüşü artışı geçiş bölgesinde %30 olarak ölçülmüştür.

TABLE OF CONTENTS

ACKNOWLEDGEMENTS	iii
ABSTRACT	iv
ÖZET	v
LIST OF FIGURES	viii
LIST OF TABLES	xi
LIST OF SYMBOLS	xii
LIST OF ACRONYMS/ABBREVIATIONS	xiv
1. INTRODUCTION	1
1.1. Problem Overview	1
1.2. Literature Survey	2
1.2.1. Nanofluid Synthesis and Colloidal Stability	2
1.2.2. Thermal Conductivity and Rheological Behavior of Nanofluids	3
1.2.3. Graphene-based Nanofluids	6
1.2.4. Convective Heat Transfer and Pressure Drop of Nanofluids	8
1.3. Objectives	10
2. METHODOLOGY	12
2.1. Nanofluid Preparation	12
2.2. Characterization Methods	14
2.2.1. Morphological Characterization	14
2.2.2. Material Characterization	15
2.2.3. Stability Characterization	15
2.2.4. Rheological Characterization	16
2.2.5. Thermal Characterization	17
2.3. Convective Heat Transfer Measurements	18
2.4. Data Reduction	21
2.4.1. Uncertainty Analysis	26
3. RESULTS AND DISCUSSION	29
3.1. Morphological Characterization	29

3.2. Material Characterization	31
3.3. Stability Characterization	31
3.4. Rheological Characterization	32
3.5. Thermal Characterization	39
3.6. Thermophysical Property Comparison with Literature	40
3.7. Forced Convection in Nanofluids	40
3.7.1. Pressure Drop and Friction Factor	40
3.7.2. Heat Transfer Coefficient and Nusselt Number	44
4. CONCLUSION AND FUTURE WORK	54
4.1. Conclusion	54
4.2. Recommendations for Future Work	56
REFERENCES	57
APPENDIX A: ESEM IMAGES OF DRY GRAPHENE NANOPARTICLES .	69
APPENDIX B: STEM IMAGES OF GRAPHENE-WATER NANOFUIDS .	70
APPENDIX C: CONVECTIVE HEAT TRANSFER DATA SET FOR WATER AT A REYNOLDS NUMBER OF 1400	73

LIST OF FIGURES

Figure 1.1.	Most common stabilization mechanisms: (a) electrostatic stabilization, (b) steric stabilization	3
Figure 1.2.	Structure of the fullerene, carbon nanotube and graphene nanolayers	7
Figure 2.1.	Graphene-water nanofluid preparation process: (a) weighing, (b) mechanical mixing, (c) ultrasonication, (d) prepared nanofluid . . .	13
Figure 2.2.	Zeta potential and DLS measuring device	16
Figure 2.3.	Viscosity measuring device	17
Figure 2.4.	Thermal conductivity measuring device	18
Figure 2.5.	Schematic of the experimental set-up	19
Figure 2.6.	Front view of the experimental set-up	20
Figure 2.7.	Section view of the experimental set-up	21
Figure 2.8.	Relative uncertainty of h_x and Nu_x along the test tube	27
Figure 3.1.	ESEM images of dry graphene nanoparticles	29
Figure 3.2.	STEM images of graphene-water nanofluids for different mass concentrations (a) 1%, (b) 0.5% with the scales $2\mu\text{m}$ and 500 nm respectively	30

Figure 3.3.	Particle size distribution of graphene-water nanofluid by DLS measurements	30
Figure 3.4.	Raman spectrum of the graphene nanosheets	31
Figure 3.5.	Change of the viscosity with respect to the concentration at 25°C	33
Figure 3.6.	Absolute viscosity change with temperature	34
Figure 3.7.	Relative viscosity change with temperature	35
Figure 3.8.	Relative viscosity variation with respect to the different shear rates at 25°C	36
Figure 3.9.	Hysteresis analysis of the graphene/water nanofluids for different particle mass fractions (a) 0.1%, (b) 0.5%, (c) 1.0%, (d) 1.5%, (e) 2.0% (lines with → indicates the measurements increasing shear rate cases, and lines with ← indicates the decreasing shear rates) .	39
Figure 3.10.	Relative thermal conductivity of graphene-water nanofluids at 25°C	40
Figure 3.11.	Pressure drop change for different concentrations and flow rates .	42
Figure 3.12.	Friction factor change trends for laminar, transition and turbulent flow	43
Figure 3.13.	Comparison of local heat transfer coefficient measurements with Shah and London correlation for DI water at $Re_D=1400$ and 1960	45
Figure 3.14.	Comparison of mean heat transfer coefficient measurements with Gnielinski correlations for DI water	45

Figure 3.15.	Local heat transfer coefficient of graphene-water nanofluids for 0.025, 0.1 and 0.2% mass concentration at $Re_D \approx 1400$ and $Re_D \approx 1950$. . .	46
Figure 3.16.	Relative thermal conductivity and viscosity of graphene-water nanofluids for 0.025, 0.1 and 0.2% mass concentration	48
Figure 3.17.	Local Nusselt number of graphene-water nanofluids for 0.025, 0.1 and 0.2% mass fraction	49
Figure 3.18.	Mean heat transfer coefficient change of graphene-water nanofluids for 0.025, 0.1 and 0.2% mass concentration	50
Figure 3.19.	Mean heat transfer coefficient change trends of graphene-water nanofluids with 0.025, 0.1 and 0.2% mass concentration for laminar, transition and turbulent flow	51
Figure 3.20.	Mean Nusselt number change of graphene-water nanofluids for 0.025, 0.1 and 0.2% mass concentration	52
Figure A.1.	ESEM images of dry graphene nanoparticles in different scales . . .	69
Figure B.1.	STEM images of graphene-water nanofluids with the particle mass concentration of 0.1% in different scales	70
Figure B.2.	STEM images of graphene-water nanofluids with the particle mass concentration of 0.5% in different scales	71
Figure B.3.	STEM images of graphene-water nanofluids with the particle mass concentration of 1% in different scales	72

LIST OF TABLES

Table 3.1.	Zeta potential values with respect to different nanoparticle-PVP ratios	32
Table 3.2.	Thermo-physical property comparison of different graphene/surfactant solutions in the literature	41
Table 3.3.	Approximate onset of the transition and turbulence regimes in terms of Reynolds number according to pressure drop measurement . . .	44
Table 3.4.	Local heat transfer coefficient increase of graphene-water nanofluids for $Re_D \approx 1400$ and 1950 at $x/D = 120$ and $x/D = 240$	47
Table 3.5.	Approximate onset of the transition and turbulent flow regimes in terms of Reynolds number according to heat transfer measurements	49
Table C.1.	The parameters used in the heat transfer calculations for water at $Re_D = 1400$	73
Table C.2.	Measured wall and inlet temperatures, and local heat transfer coefficients along the test pipe for DI water at $Re_D = 1400$	74

LIST OF SYMBOLS

bf	Base fluid (Subscript)
c_p	Heat capacity of fluid
D	Hydraulic diameter of pipe
f	Friction factor
\bar{h}_D	Mean convective heat transfer coefficient
h_x	Local convective heat transfer coefficient
I	Intensity ratio
k	Thermal conductivity coefficient
L	Test section length
\dot{m}	Mass flow rate
nf	Nanofluid (Subscript)
np	Nanoparticle (Subscript)
Nu_x	Local Nusselt number
\overline{Nu}_D	Mean Nusselt number
P_1	Fluid pressure at the inlet
P_2	Fluid pressure at the outlet
Pr	Prandtl number
PSIG	Pounds per square inch gauge
q''	Heat flux applied to test section
q_f	Heat transferred to system from heater
q_{in}	Power supplied to heater
Re_D	Reynolds number
\bar{T}_w	Average temperature of the thermocouples mounted on pipe
\bar{T}_f	Average of the inlet and outlet temperatures
$T_{m,i}$	Fluid inlet mean temperature
$T_{m,o}$	Fluid outlet mean temperature
$T_m(x)$	Local mean fluid temperature
$T_w(x)$	Local wall temperature

u_m	Mean fluid velocity
x	Axial distance from heated part of the test section
x^*	Dimensionless axial distance
ΔP	Pressure drop along the test section
ϕ	Particle mass concentration
μ	Dynamic viscosity
ρ	Density
π	Pi number
$\sigma_{\Delta P}$	Uncertainty of pressure drop
σ_f	Uncertainty of friction factor
σ_h	Uncertainty of convective heat transfer coefficient
σ_{Nu}	Uncertainty of Nusselt number
$\sigma_{q''}$	Uncertainty of heat flux

LIST OF ACRONYMS/ABBREVIATIONS

ASTM	American Society for Testing and Materials
CNT	Carbon nanotube
CTAB	Cetyl trimethyl ammonium bromide
DI	De-ionized
DLS	Dynamic light scattering
DTAB	Dodecyl trimethyl ammonium bromide
EG	Ethylene glycol
ESEM	Environmental scanning electron microscopy
f-GNP	Functionalized graphene nanoplatelet
f-HEG	Functionalized hydrogen exfoliated graphene
GA	Gum arabic
GO	Graphene oxide
GnP	Graphene nanoplatelet
GnS	Graphene nanosheet
MWCNT	Multi-walled carbon nanotube
PVP	Polyvinyl pyrrolidone
SDBS	Sodium dodecyl benzene sulfonate
SDS	Sodium dodecyl sulfate
STEM	Scanning transmission electron microscopy
TA	Tannic acid
THW	Transient hot-wire

1. INTRODUCTION

1.1. Problem Overview

Efficient energy transport is critical for many engineering applications such as chemical processes, thermal management and energy systems. Water, ethylene glycol (EG) and propylene glycol are the most common heat transfer fluids used in these industries and have limited thermo-physical properties. Therefore, researchers have been investigating the alternative ways to improve the thermo-physical properties of these heat transfer fluids. Micron and millimeter-sized particles were added into a liquid to enhance the heat transfer properties. However, the colloidal stability of the solutions was not good and solid particles precipitated after a while, leading to sedimentation, agglomeration, clogging problems and as a result, high-pressure drop in the applications [1]. With the developments of nanotechnology, Choi suggested the use of nanometer-sized particles in 1995 [2], and a new era for heat transfer fluids have begun with the invention of so-called nanofluids. It was shown that nanometer-sized particles dispersed into a base fluid increases the thermal conductivity, with acceptable stability due to the high surface area to volume ratio of nano-sized particles [3]. Researchers observed significant heat transfer enhancement for a wide range of applications by using nanofluids containing nanoparticles such as SiO_2 , Al_2O_3 , CuO , TiO_2 , Fe_2O_3 and some carbon forms [4].

Nanofluids have been considered as the next generation heat transfer fluids due to their enhanced thermal features. However, there are still some challenges regarding with the stability and increased viscosity. Because sedimentation directly affects the continuity of the applications, it is a major drawback of the nanofluids. Researchers have been trying to prepare solid-liquid suspensions that have long term stability since the concept was introduced. Another challenge is the increase in viscosity that decreases the system efficiency by increasing pressure drop. Nanoparticles added into a liquid increase its thermal conductivity, but the viscosity of the mixture increases as

well. Balancing between viscosity and thermal conductivity has great importance for optimizing the amount of nanoparticles added. Therefore, rheological characterization of nanofluids is required before using them for various applications.

In addition to thermo-physical characterization, the convective heat transfer behavior of the nanofluids should also be investigated. Hence, researchers tested nanofluid samples in different concentrations, temperatures and flow rates and investigated their effects on heat transfer. Even though many studies investigated the nanofluids under different flow regimes, most of them focused on laminar and turbulent region. The heat transport behavior in the laminar to turbulence transition still has many uncertainties, so this topic should be clarified for nanofluids to be considered a reliable heat transfer fluid.

1.2. Literature Survey

1.2.1. Nanofluid Synthesis and Colloidal Stability

The experimental results of the nanofluids should be verifiable when the same preparation method is performed. Therefore, some methods have been developed to eliminate the inconsistencies between different studies. One-step and two-step methods are the most common approaches for nanofluid preparation. In the one-step method, a nanofluid is prepared simultaneously synthesizing the nanoparticles and dispersing them in the base fluid [5]. In the two-step method, nanoparticles are produced by physical or chemical methods first, then added into the base fluid for preparing the nanofluid. A well-mixed dispersion is obtained by applying some processes such as high-shear mixing, ultrasonication, magnetic stirring, homogenizing and ball milling after nanoparticles added [5, 6]. Since the two-step method allows to produce large amounts of nanofluids and easy applicable, it is the most common method for preparing nanofluids. However, strong van der Waals forces and surface charges among nanoparticles lead to agglomerations that affect the stability and heat transfer characteristics

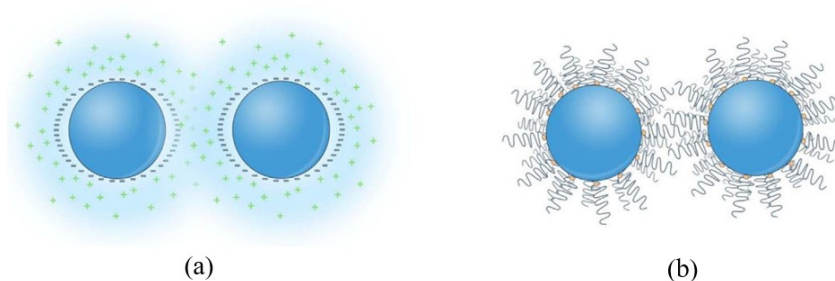


Figure 1.1. Most common stabilization mechanisms: (a) electrostatic stabilization, (b) steric stabilization [10]

of the nanofluid in this method [7]. Some techniques such as using surface-active materials (or surfactants), pH control and using functionalized nanoparticles have been used to overcome the agglomeration and stability problems in nanofluids.

The stability of nanofluids is based on the balance between attractive and repulsive forces among nanoparticles. Nanoparticles are well dispersed if the repulsive forces are dominant, this leads to colloidal stability. The stability of nanofluids can be achieved by electrostatic (Figure 1.1a) and steric stabilization (Figure 1.1b) mechanisms. Steric stabilization is obtained by surfactants and it has some advantages over electrostatic stabilization as electrostatic stabilization might necessitate suspensions being significantly acidic or basic that might have negative impact on equipment reliability. Surfactants in an organic structure comprise of hydrophobic tail and hydrophilic head [8]. As it is shown in the Figure 1.1b, the heads of the surfactants stick on the surface of the nanoparticles, whereas the tails prevent agglomerations in the suspension by pushing other nanoparticles [8–10].

1.2.2. Thermal Conductivity and Rheological Behavior of Nanofluids

Nanofluids provide an anomalous heat transfer augmentation in comparison to conventional heat transfer fluids due to their unique heat transfer mechanisms. The observed anomalous heat transfer increase of nanofluids is attributed to several mechanisms including Brownian motion, nano-layering of the liquid molecules at the particle interfaces, and percolation through clustering nanoparticles [11]. The Brownian

motion is argued to be an important mechanism for heat transfer enhancement that is based on the stochastic movements of nanoparticles in a liquid leading to micro-convection effects [12,13]. The nanolayer bridges the nanoparticle and liquid to create a uninterrupted thermal profile leading to a remarkable increase compared to classical models [14]. Nanoparticle clustering or percolation networks are proposed as another possible mechanism for nanoscale heat transfer. Low-level nanoparticle clustering is considered as the most important mechanism leading to the anomalous thermal conductivity augmentation [15]. The regions that nanoparticles intensively contained in a liquid have higher thermal conductivity than liquid dominant ones. [16].

Many nanoparticles such as aluminum oxide (Al_2O_3), copper oxide (CuO), titanium dioxide (TiO_2), zinc oxide (ZnO), ferrimagnetic (Fe_3O_4 and Fe_2O_3) and carbon-based (graphite, CNT, graphene) have been used to prepare nanofluids. Since each has distinct properties, their potential in different applications can be determined based on different thermo-physical properties. For instance, carbon-based nanofluids are appropriate for solar applications due to their superior thermal conductivity and absorption properties, whereas zinc oxide-based nanofluids can be used in the electronics industry because of their catalytic and optoelectronic properties. Also, concentration, nanoparticle size and shape, pH and temperature are influential on the thermo-physical properties of nanofluids [4], that can be determined by characterizing nanofluids. Thermal conductivity and viscosity are two important properties regarding to heat transport, so many studies focused on these in the literature. Chon *et al.* [17] studied Al_2O_3 -water nanofluids with different nanoparticle sizes with 1% volume concentration, and they found 22% conductivity enhancement for 11-nm nanoparticles at 71 °C. Their results showed that the thermal conductivity enhancement increases with decreasing the particle size. Das *et al.* [18] investigated the water-based Al_2O_3 and CuO nanofluids for the volume fraction of 4% and observed up to 26% and 28% thermal conductivity enhancement respectively. Also, they reported that there is a strong dependency between temperature and thermal conductivity for both nanofluids. When the temperature of the nanofluid is increased from 21 to 51 °C, they monitored significant enhancement in

thermal conductivity. Duangthongsuk and Wongwises [19] observed thermal conductivity augmentation of 3-7% for TiO₂-water nanofluids in a broad volume concentration range (from 0.2 to 2%). Jeong *et al.* [20] studied particle shape effect for the ZnO-water nanofluids and showed thermal conductivity of rectangular particle based nanofluids is higher than spherical. Ding *et al.* [21] observed 8 times higher thermal conductivity enhancement when the temperature of the CNT-water nanofluid increases from 20 to 30 °C. Abareishi *et al.* [22] studied with magnetic nanoparticles, Fe₃O₄, and they stated about 8% increase in thermal conductivity for 1% particle volume fraction.

Rheological behavior of the heat transfer fluids is also important since the viscosity increases by the adding solid nanoparticles into a fluid. Viscosity directly affects the pressure drop and the pumping power in the systems and it can be critical for some applications [23]. There are many experimental studies using different nanoparticles to investigate the viscosity of nanofluids. Chandrasekar *et al.* [24] studied Al₂O₃-water nanofluids with particle volume concentrations of 0.33 to 5%. Their results indicate that the viscosity of the Al₂O₃ nanofluids shows a linear increase with the particle volume fraction to 2%, followed by a nonlinear increase for higher particle volume fractions. Nguyen *et al.* [25] investigated water based Al₂O₃ and CuO nanofluids and observed significant temperature and particle volume fraction dependence of viscosity. Their results showed the relative viscosity of both Al₂O₃ and CuO nanofluids does not change too much with temperature for particle volume fractions below 4%, whereas temperature dependence was observed for higher fractions. Moreover, the reported relative viscosity is significantly higher for CuO nanofluids in comparison to Al₂O₃ nanofluids for relatively higher particle volume fractions such as 9%. Abarashi *et al.* [22] investigated the rheological behavior of magnetic α -Fe₂O₃-glycerol nanofluids, and observed shear thinning characteristics. Duangthongsuk and Wongwises [19] investigated the TiO₂-water nanofluids, and found that the classical viscosity models were not in agreement with their experimental results. Phuoc *et al.* [26] experimentally studied multi-walled carbon nanotube (MWCNT)-water nanofluids and reported Newtonian behavior for low-concentrated samples (0.24-1.43%), whereas that shear thinning behavior observed for higher particle volume concentrations.

Some researchers reported that the nanofluids might exhibit hysteresis behavior under various circumstances and analyzing the hysteresis is important due to its direct effect on the pumping power and energy consumption for highly transient operations and applications. Nguyen et al. [27] studied Al₂O₃-water and CuO-water nanofluids and reported different behavior following heating and cooling processes. They observed hysteresis once a critical temperature and particle volume fraction is exceeded. Jiang et al. [28] investigated the viscosity and hysteresis behavior of ammonia/water nanofluids by using different nanoparticles and they proposed that the surfactants' molecular structure might be altered at higher temperatures, affecting its functionality leading to particle aggregation and sedimentation. Thus, they explained observed hysteresis by the changing morphology. Rather than focusing on changing temperature, Aladag et al. [29] investigated the hysteresis phenomena for water based Al₂O₃ and CTN nanofluids by measuring the viscosity while increasing and decreasing the shear rates. They showed that the shear stress for increasing shear rates is higher than it is for decreasing rates and hysteresis is observed for both nanofluids due to the disintegration of agglomerated particles with increasing shear rates.

1.2.3. Graphene-based Nanofluids

Recently, using directional materials for producing nanofluids such as graphite [30], boron nitride [7] and CNT [31] have received increasing interest due to the observed remarkable properties. Graphene, which is comprised of a single/few hexagonal sheet(s) of covalently bonded carbon atoms have been receiving significant interest since it was presented by Novoselov *et al.* [32]. The structures of the graphitic forms carbons, fullorene, nanotube and graphene nanolayers, are shown in Figure 1.2. Graphene layers are fabricated by exfoliating three dimensional graphite. High thermal and electrical conductivity, high carrier mobility, long-range ballistic transport at room temperature, high Young's modulus and fracture strength are some of its outstanding properties [33]. Balandin *et al.* [34] reported the thermal conductivity of graphene as 5000 W/m.K that is superior to that CNT's, making it a promising material for producing nanofluids.

There have been recent studies focusing on the production and properties of graphene nanofluids. Yu *et al.* [36] prepared graphene oxide (GO)-EG nanofluids and obtained 61% conductivity enhancement for 5% volume concentration. Baby and Ramaprabhu [3] investigated 0.056% particle volume fraction graphene-water nanofluid and observed 14% augmentation of thermal conductivity. Yu *et al.* [37] observed 86% enhancement for graphene (GnS)-(EG) nanofluid with 5% particle volume fraction. Gupta *et al.* [38] reported strong temperature dependence for GnS-water nanofluids unlike CNT nanofluids. The enhancement in thermal conductivity of GnS-water nanofluids is 17% with the temperature increase of 20°C. Mehrali *et al.* [39] studied nanofluids with graphene nano-platelets with different surface areas and they reported that the largest thermal conductivity augmentation is 27%, achieved using the nano-platelets with the highest surface area. They also observed 44% increase in viscosity for 0.1% particle mass fraction. Hajjar *et al.* [40] prepared graphene oxide (GO)-water nanofluids and reported significant effect temperature on thermal conductivity enhancement, with 34% and 47% increase in thermal conductivity at 20°C and 40°C, respectively for 0.25% particle mass fraction. Ghozatloo *et al.* [41] investigated the

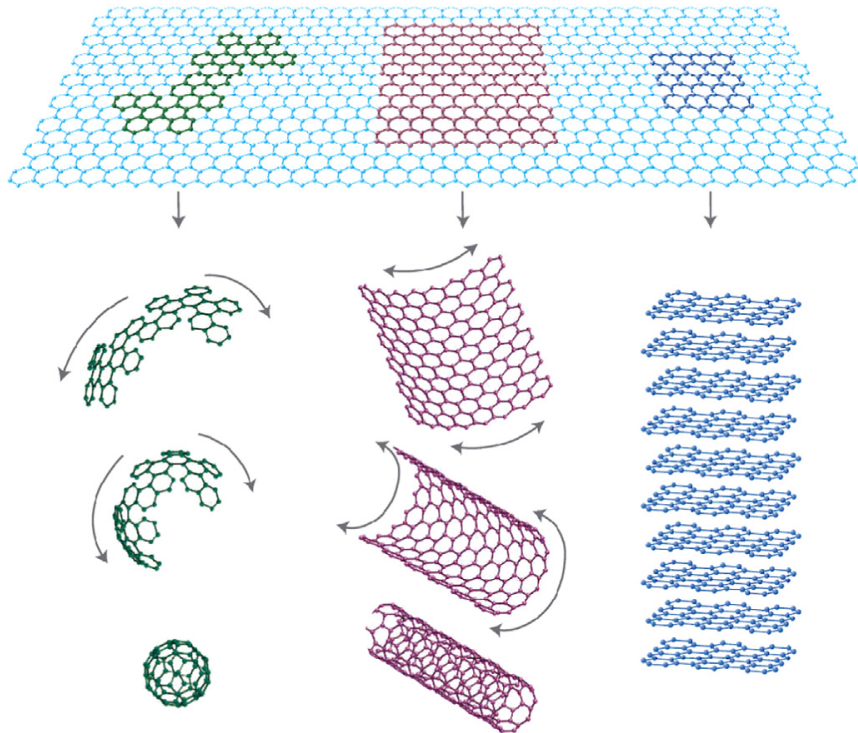


Figure 1.2. Structure of the fullerene, carbon nanotube and graphene nanolayers [35]

time and temperature effect on thermal conductivity of graphene-water nanofluids. The enhancement is 17% for 0.03% mass concentrated sample at 50°C, whereas it is 12.5% at 25°C. Thermal conductivity of the nanofluids decreased a little in the first 45 hours, then it remained constant. Kole *et al.* [33] observed observed remarkable viscosity increase, which is almost 100% for 0.395% particle volume fraction and about 15% augmentation of thermal conductivity with functionalized hydrogen exfoliated graphene (f-HEG)-water nanofluid. Moghaddam *et al.* [42] observed that viscosity of the graphene-glycerol nanofluids increases 300% with respect to that of the base fluid for 2% particle concentration. Moreover, the nanofluid exhibits shear thinning behavior, even though the base fluid is Newtonian. Sarsam *et al.* [43] prepared functionalized graphene nanofluids by using different surfactants, and reported 3-21% higher viscosity for their nanofluids. Recently, Yang *et al.* [44] studied the GO-water nanofluids with different temperatures and concentrations. They reported thermal conductivity enhancement of 48% for the particle mass fraction of 1.5% at 60°C and the enhancement increases with temperature due to the Brownian motion.

1.2.4. Convective Heat Transfer and Pressure Drop of Nanofluids

Convective heat transfer performance and flow behavior of nanofluids under different flow regimes have also been an area of interest for researchers. Most of them observed significant heat transfer enhancement for different nanoparticles even though some researchers reported little or no enhancement. Heyhat *et al.* [45] investigated the thermophysical properties and convective heat transfer of Al₂O₃-water nanofluids under laminar flow regime for particle volume fractions 0.1 to 2%. They observed 3% heat transfer enhancement for 0.1% volume fraction at a Reynolds number of 330, whereas the enhancement increased to 32% for the 2% volume fraction at a Reynolds number of 2100. They also reported up to 6 times higher pressure drop compared to that of water. Pak and Cho [46] studied convective heat transfer of Al₂O₃-water and TiO₂-water nanofluids in a circular pipe, subject to a constant heat flux under turbulent regime. They showed that heat transfer coefficient for 3% volume concentration nanofluid is 12% lower than that of pure water even though the Nusselt number

increases with Reynolds number and volume fraction. Heris *et al.* [47] observed that the heat transfer performance of CuO-water nanofluids under laminar regime is remarkably better than pure water, and stated that the heat transfer enhancement is more apparent especially in the higher Reynolds numbers. Fotukian and Esfahany [48] also studied with CuO-water nanofluids, but under turbulent flow conditions and at lower nanoparticle concentrations. Convective heat transfer enhancement they report is 25% and pressure drop increase is 20% for 0.03% particle volume fraction. Kayhani *et al.* [49] investigated TiO₂-water nanofluids under turbulent flow regime and constant heat flux boundary conditions. Their results showed that the added TiO₂ nanoparticles lead to moderate augmentation in heat transfer with Nusselt number increasing 8% for 2% particle volume concentration at a Reynolds number of 11780. Whereas, they did not observe an abnormal increase in the pressure drop in comparison to that of water. Hemmat Esfe *et al.* [50] observed a heat transfer enhancement up to 12% for Ag-water nanofluids with low particle concentrations and under turbulent regime and the increase in pressure drop is about 16%.

In addition to the metallic and ceramic nanoparticles, carbon-based nanoparticles have been widely used in recent years to produce nanofluids. Wang *et al.* [51] investigated the heat transfer behavior of multiwalled carbon nanotube (MWCNT)-water nanofluids in a horizontal circular tube under laminar flow regime, and showed that there is a significant enhancement in heat transfer up to 190% even at low Reynolds numbers such as 120. They also observed a linear increasing trend in the pressure drop with respect to Reynolds number. Baby and Ramaprabhu [52] prepared nanofluids by dispersing f-HEG nanoparticles into EG/water mixture and investigated the convective heat transfer performance under turbulent flow regime. They measured entrance and developed heat transfer enhancements separately; their results showed that f-HEG dispersed nanofluid for 0.01% particle volume fraction increased the heat transfer up to 170% at the entrance, whereas the enhancement is around 140% at outlet of the pipe. Ghozatloo *et al.* [53] studied graphene-water nanofluids focusing on the thermal characterization under laminar regime. The relationship between convective heat transfer, temperature and concentration is investigated and remarkable heat

transfer enhancement is observed by increasing temperature or concentration. When the mass concentration of the nanofluids is increased from 0.025 to 0.1%, they observed 15% heat transfer increase at 25°C, but it is 24% at 38°C. So, they stated that the effect of increasing temperature is more significant than concentration. Akhavan-Zanjani *et al.* [54] investigated the convective behavior of graphene-water nanofluids under laminar flow in a uniformly heated circular pipe, and reported heat transfer enhancement of about 14% for 0.02% particle volume fraction at a Reynolds number of 1850. Selvam *et al.* [55] investigated the convective heat transfer characteristics of graphene-water/EG nanofluids for 0.1-0.5% particle volume concentration in a broad range of Reynolds number. They observed up to 170% enhancement in heat transfer coefficient at a Reynolds number of 6790 and 96% enhancement in Nusselt number. Yarmand *et al.* [56] studied the heat transfer coefficient and pressure drop of functionalized graphene nanoplatelet (f-GNP)-water nanofluid in a square duct. They observed that the enhancement of heat transfer coefficient and Nusselt number are 19% and 26% respectively for 0.1% particle mass fraction. The friction factor of the nanofluid increases 9% in comparison to water at a Reynolds number 17500.

1.3. Objectives

There has been an increasing number of studies about the characterization of graphene nanofluids in recent literature. While most of these are dedicated to the thermal transport properties, only very few focus on the rheological behavior, and they consider only a limited range of concentration. Moreover, no studies are investigating the hysteresis behavior in graphene nanofluids. A preparation recipe for graphene nanofluids is developed, and morphological, thermal and rheological characterization of the graphene nanofluids are experimentally carried out in this study. While the thermal and stability features of the produced graphene nanofluids are presented; the rheological behavior is emphasized. It must be highlighted that hysteresis in measured viscosity for graphene-water nanofluids is investigated for the first time in this study. Furthermore, most of the studies in the literature investigate the thermo-physical properties of graphene nanofluids for low concentrations. Understanding the flow behavior

of the graphene-water nanofluids in higher concentrations will be more important with the nanoparticle production become cheaper in the future. Hence, relatively higher concentrations up to 2% particle mass fractions are studied and reported, expanding the range in the existing literature.

In addition to thermo-physical characterization of the graphene-water nanofluids, convective heat transfer investigation is also carried out. Even though there are limited number of studies regarding the transitional flow behavior of some metallic and ceramic nanoparticles, such as Al_2O_3 , ZnO and Cu , no studies reporting the transitional behavior of graphene dispersed nanofluids. Convective heat transfer behavior and pressure drop characteristics of the graphene-water nanofluids are investigated experimentally by focusing on the transition from laminar to turbulent flows. The graphene-water nanofluids having the particle mass fractions of up to 0.2% are considered. Since the reliability of the test system and the measurement results would be questionable in the higher concentrations, convective heat transfer behavior is investigated for relatively lower particle concentrations. The effect of particle concentration to the laminar to turbulence transition point is examined together with its effect on heat transfer and pressure drop.

2. METHODOLOGY

2.1. Nanofluid Preparation

Graphene-water nanofluids are prepared by the two-step method in this research. The purchased nanoparticles are mixed into de-ionized (DI) water that is used as base fluid. Graphene nanoplatelets used are reported to have 5-10 nm thickness, 5-10 μm lateral size and 99% purity (Grafen Chemical Industries, Turkey). Graphene is hydrophobic and it does not disperse in polar solvents such as water. Steric stabilization is preferred in this study due to its advantages over electrostatic stabilization. Surface active materials are added into the base fluid prior to mixing of the nano-flakes to achieve stable suspensions. Three types of surfactant groups, anionic (i.e. SDS, SDBS, GA etc.), cationic (i.e. CTAB and DTAB), and non-ionic (i.e. Triton X-100, TA and PVP), can be used in nanofluid dispersions [57]. Being an organic material, using GA might support micro-organism growth leading to mold formation limiting long term usability. Using SDS leads to foaming [7], which is not desired for heat transfer applications. Whereas, SDBS properties change, after it is exposed to higher temperatures [28]. For this reason, steric stabilization for the graphene-water nanofluids is recommended by using non-ionic surfactants [58, 59]. Yoon and In [60] stated that hydrophobic interaction between reduced graphene nanoplatelets and PVP ensures high solubility. Zhao *et al.* [61] also used PVP as a surfactant in their graphene-water nanofluid study and they achieved stable solutions after 1 month from preparation. Besides, the properties of nanofluids prepared using PVP do not change after it is subject to higher temperatures [62]. Hence, polyvinyl pyrrolidone (PVP K30) is used as a surface active material in this study.

The surface active material, PVP K30, is weighed by precision scale (Kern PFB, ± 10 mg), added to 100 ml DI-water, and stirred by a mechanical mixer (Heidolph, RZR 2021) for 15 minutes at 1600 rpm until the surfactant-water solution becomes homogenous. Graphene nano-flakes are then introduced into the solution and they are

mechanically mixed for 45 minutes at 1600 rpm. The suspension is then subjected to ultrasonic mixing (Hielscher UP400S, using sonotrode H22) for 2 hours with 200 W, where it is placed into a water bath to prevent overheating and vaporization the fluid. The temperature of the bath is set to 8 °C by using a temperature controlled a circulating chiller (PolyScience 9106A12E). The preparation process is shown in the Figure 2.1.

The PVP and graphene concentrations of the suspensions are reported as mass fractions as definition of volume for graphene nano-flakes is ambiguous. The preparation recipe presented is identified as a result of an optimization study to achieve long

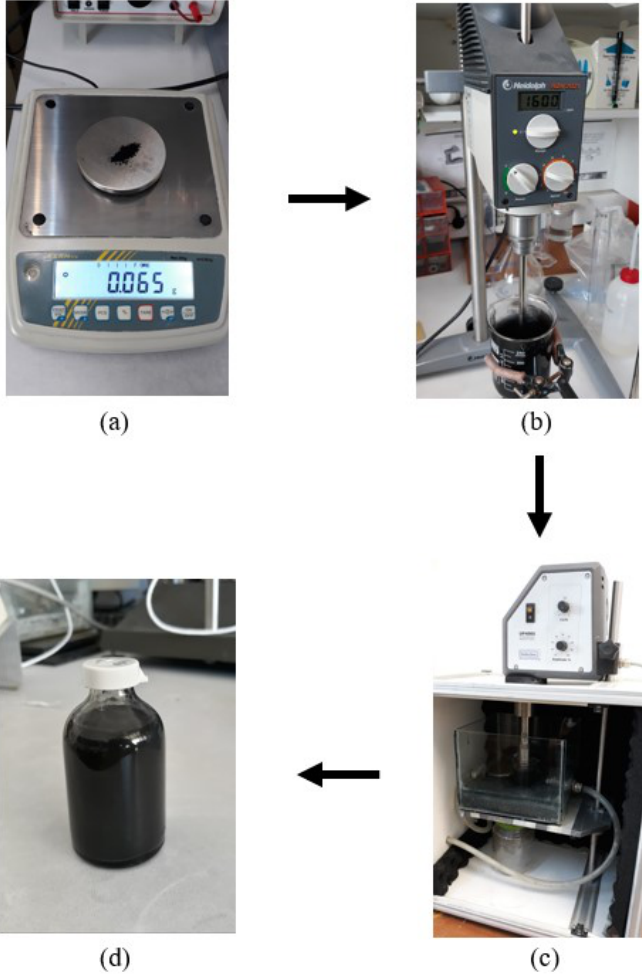


Figure 2.1. Graphene-water nanofluid preparation process: (a) weighing, (b) mechanical mixing, (c) ultrasonication, (d) prepared nanofluid

term stability using minimum amount of surface active material so that the viscosity will not be increased significantly due to the addition of surface active material. Graphene mass fractions that are considered in this study vary from 0.1 to and 2%, whereas PVP concentrations are adjusted depending on the graphene's fraction and vary from 0.1 to 2% based on the results of the optimization study.

2.2. Characterization Methods

The produced nanofluids are characterized to examine their morphology and identify their thermophysical properties. Morphological characterization is carried out by visual characterization methods such as environmental scanning electron microscopy (ESEM), and scanning transmission electron microscopy (STEM) imaging and dynamic light scattering (DLS). Raman spectroscopy is used for material characterization and stability assessment is carried out by zeta potential measurements. Finally, thermal conductivity and viscosity are measured for identifying the thermo-physical behavior of the produced nanofluids.

2.2.1. Morphological Characterization

Imaging the produced nanofluids using an electron microscope helps to identify the morphological structure, and observing the particle agglomeration level of the suspensions. Besides, these imaging techniques also help to confirm the manufacturer reported size of the particles before the mixing process. Firstly, ESEM images of the dry particles are captured by transmission scanning electron microscope (Philips XL30 ESEM-FEG/EDAX) to characterize the dry nanoparticle size. Then, STEM imaging is used with the same instrument to observe the morphological structures of the particles and aggregates within the nanofluid. For that, nanofluid samples with different concentrations are diluted to 0.01% particle mass fraction and dried over copper grids to get quality images. There have been taken at least 10 images by ESEM and STEM. Since all the images are consistent with each other, two of them are shown as representations. Dynamic light scattering (DLS) is a method that is used for characterizing the

particle size distribution of colloidal suspensions with sphere like particles. Although its use for characterization of colloidal suspensions of nano-flakes is questionable, it was reported that the peak of the particle size distribution measured by DLS is well correlated with the TEM measurements [63]. As a result, DLS is performed by using Malvern Zetasizer Nano ZSP for identifying the aggregate size.

2.2.2. Material Characterization

Material characterization by Raman spectroscopy is widely used to identify the doping level and quality of the material. For graphene, G and D characteristic peaks are observed around 1574 cm^{-1} and 1331 cm^{-1} , respectively [42]. The location of the G peak indicates the in-plane vibrations of sp^2 carbon atoms and the number of layers of the graphene nano-sheets can be interpreted via G peak accordingly; moves to lower frequencies as the number of layers increases. Whereas, D peak shows the disordered structure level and indicates the quality of the graphene even though its position is related to the excitation wavelength [64]. The intensity rate of the D to G peaks (I_D/I_G) implies the defect density of the graphene nanosheets [65]. In this study, Raman spectroscopy of the graphene is carried out by the Renishaw inVia Raman Microscope and 532 nm green laser is used in the experiment with an exposure time of 10 seconds.

2.2.3. Stability Characterization

Zeta potential measurements are widely utilized for assessing the stability of the colloidal suspensions. Each nanoparticle has an electric potential (or a surface charge), and the surface charge measured within the suspension is a good indicator of the stability. The measurement detects the electrophoretic mobility of the charged particles under the electrical field and suspensions that have high mobility particles resulting in high absolute value of zeta potential are considered to be stable. The zeta potential scale varies between -100 mV and 100 mV and the suspensions that have zeta potential larger than 30 mV or less than -30 mV are assumed as stable [66]. Sample

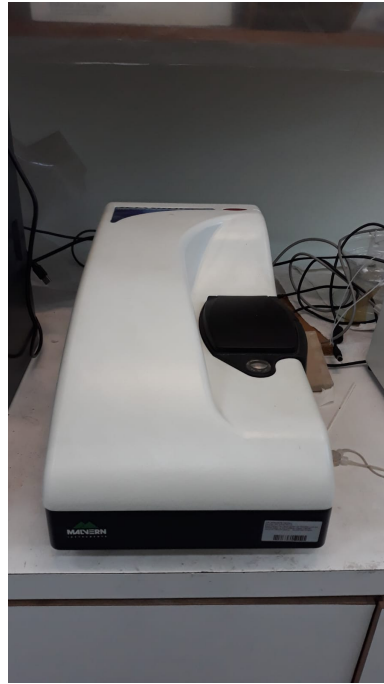


Figure 2.2. Zeta potential and DLS measuring device

nanofluids are diluted to 0.01% particle mass fraction, and zeta potential is measured by Zetasizer Nano ZSP, (Malvern Instruments, $\pm 2\%$ error). Measurements are repeated 5 times to verify the results using different samples taken from the produced suspensions.

2.2.4. Rheological Characterization

A cone-plate rheometer (Brookfield DV-III Ultra) that is shown in Fig. 2.3 is used to measure the viscosity of nanofluid using a circulating chiller (PolyScience, 9106A12E) for controlling the temperature of nanofluid during measurements. Viscosity is measured at different spindle speed rates from 375 to 1875 sec^{-1} and considering the shear rate dependence, the measurements are carried out both from low-to-high speed rates and from high-to-low speed rates to investigate hysteresis. The viscosity values of DI-water and ethylene-glycol at 25 °C are well known, and these fluids are used as calibration fluids. Results of the calibration experiments are coherent with the reported values in the literature and viscosity values of graphene-water nanofluids are



Figure 2.3. Viscosity measuring device

measured following the validation. The viscosities reported are average of 5 measurements. The relative measurement uncertainty of the rheometer is reported to be 1.0% at the specified speeds of the spindle by the manufacturer.

2.2.5. Thermal Characterization

Thermal conductivity of produced graphene-water nanofluids is measured using transient hot-wire (THW) method based on the ASTM D7896 standard [67]. A thermal conductivity analyzer (Decagon KD2 Pro, $\pm 5\%$) is used for measurements at 25 °C. As it can be seen in the Figure 2.4, the probe of the instrument (KS-1) is fully immersed into the nanofluid vessel and the analyzer is operated at low power mode to prevent convective currents. Temperature of the samples is stabilized using a water bath and a circulating chiller (PolyScience 9106A12E) during measurements. The test vessel is placed in a beaker filled with still water to provide the uniform temperature, and the beaker is placed in a water bath. The measurements are carried out 1 hour after the explained system is set to ensure thermal equilibrium. All measurements are repeated 10 times to assess the repeatability, and the mean value is reported.

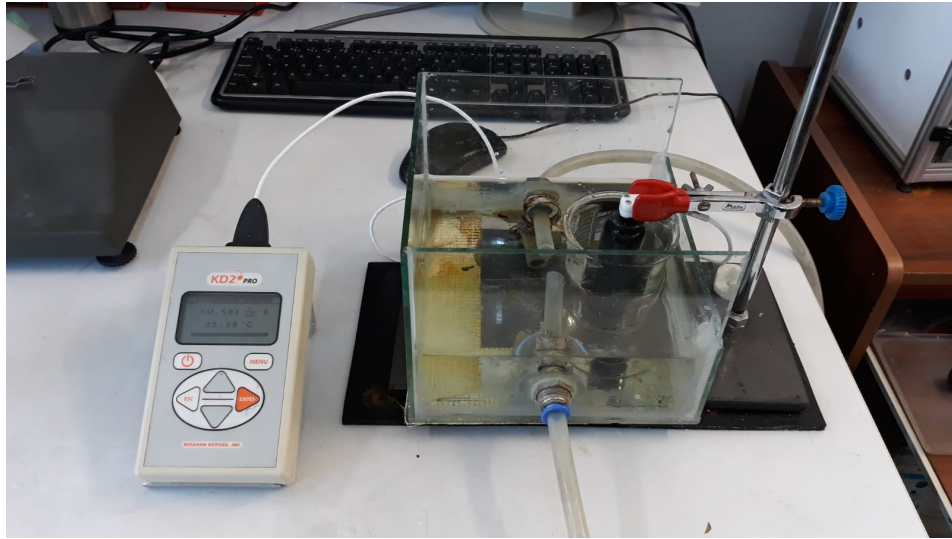


Figure 2.4. Thermal conductivity measuring device

2.3. Convective Heat Transfer Measurements

The experimental test system is built to investigate the convective heat transfer from laminar to turbulent regimes in a horizontal copper circular pipe as seen in Figures 2.5 and 2.6. Pumped fluid flows through the test section, which is comprised of a 2.1 m long circular copper pipe with 6 mm inner and 8 mm outer diameter. The first 0.6 m of the test section is not heated and is dedicated to hydrodynamic entry. Hydrodynamically developed flow enters the latter part of the test section that is heated by uniform heat flux. The test section is wrapped with the insulation layers to prevent heat removal as seen its section view in . Electrical insulation is ensured by covering the copper pipe with fiberglass sleeves with helically coiled bare nichrome heater wire wrapped on it. In order to measure the temperature on the pipe wall, thermocouples are attached to copper tube in determined axial locations. After that, heater wire is covered by zinc phosphate-based cement layer to obtain a uniform heat distribution along the pipe. Heat and electricity resistant fiber-glass insulation tape and fireproof cloth tape are wrapped on the heated section in order to prevent any ignition at high temperatures. Finally, glass wool is covered for minimizing the heat loss from the system as is seen in Figure 2.7. Heater wire is connected to AC power source at both ends and is supplied with 400 W using a potentiometer.

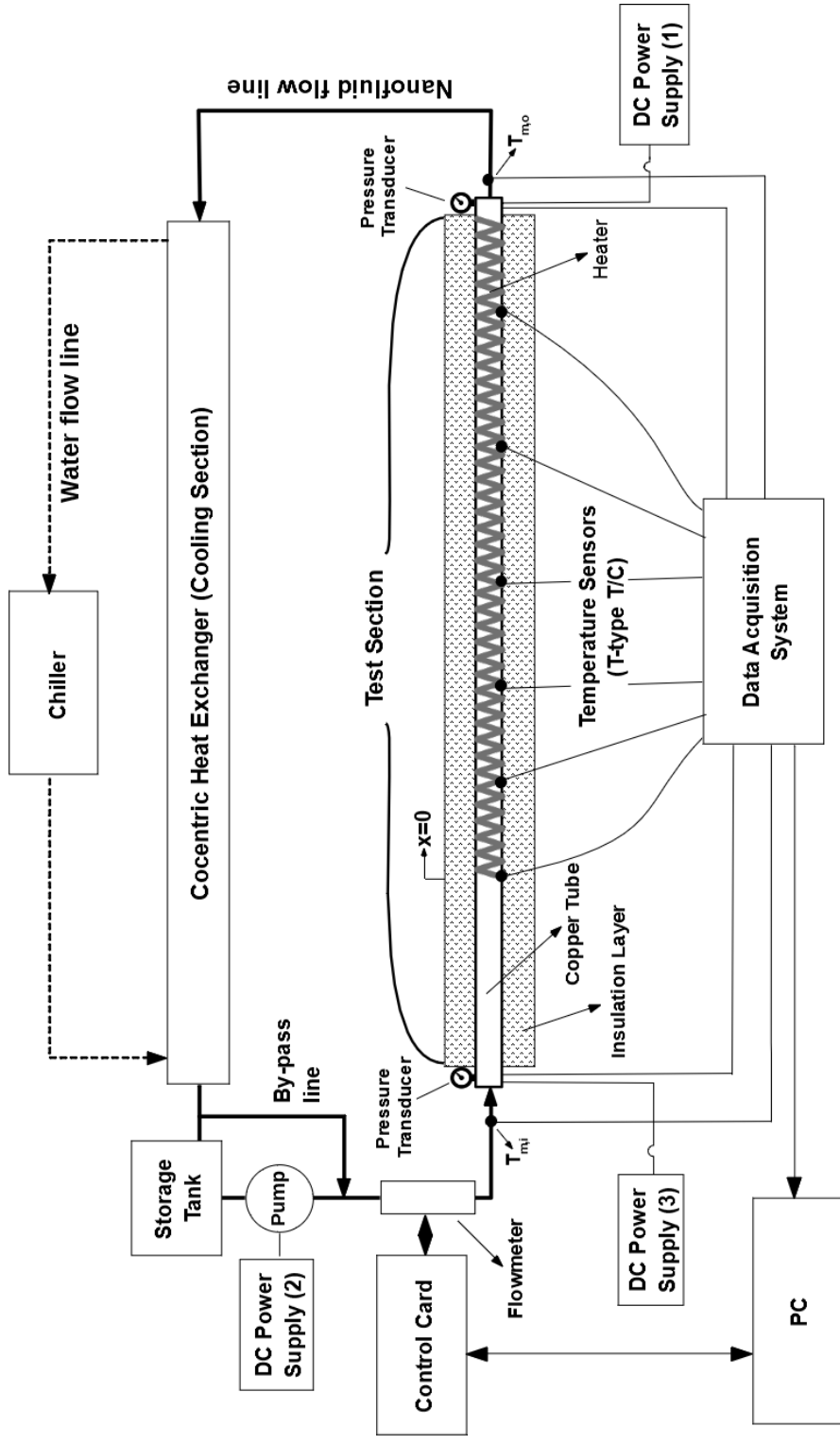


Figure 2.5. Schematic of the experimental set-up

T-type thermocouples with special error limits (Omega Inc.; $\sigma_T = \pm 0.5 \text{ }^\circ\text{C}$) are used for measuring the temperatures at different axial locations on the copper pipe. Nine thermocouples are mounted on the pipe wall at dimensionless axial locations (x/D) of 10, 33.3, 46.6, 60, 80, 100, 120, 200, 240 (starting from the heating section) and two thermocouples are inserted into the flow at the inlet and outlet of the pipe to measure the bulk mean fluid temperature. A valve-connector couple is binding right after and before the test section and in order to mix the flow and measure the mean temperature correctly. Temperature measurements are performed 1 hour after the system started circulating to ensure that steady state is reached. The measurements are collected by a data acquisition unit (Agilent 34970A). Calibration of the thermocouples is carried out by using a constant temperature water bath. The fluid exiting from the test section enters the concentric heat exchanger, where water circulated by the chiller (Polysat 12920) reduces the temperature of the fluid coming from the test section and stabilizes the temperature before enters the storage tank. The fluid is then pumped from the storage tank by a centrifugal pump (Iwaki RD-20), flow rate is adjusted by using a valve and measured by a flowmeter (Sea, YF-S402), $\sigma_m = 2\%$ of reading error. Flowmeter was calibrated before the very first experiment of this study and controlled before each experiment. Pressure drop and friction factors are calculated



Figure 2.6. Front view of the experimental set-up

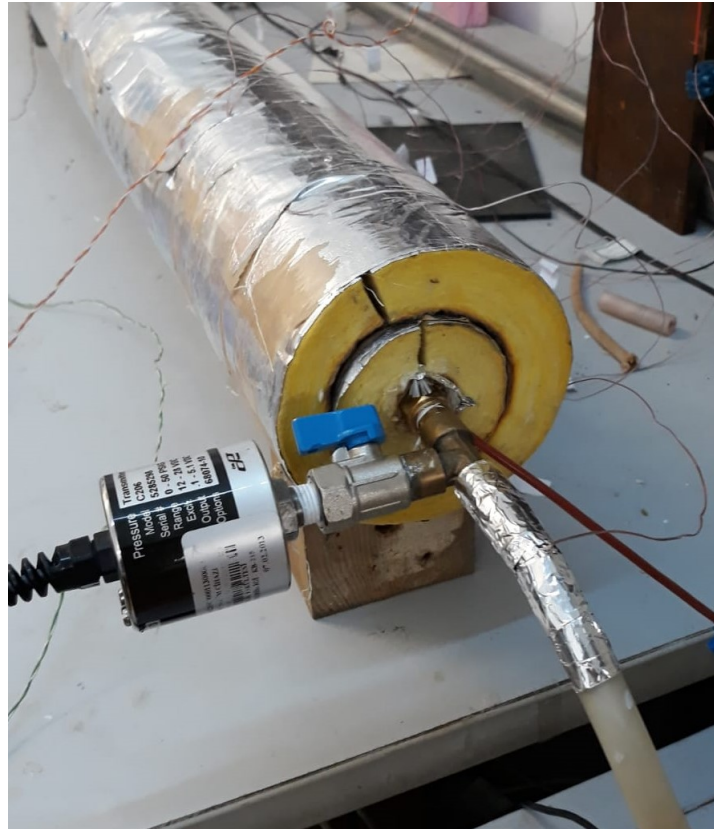


Figure 2.7. Section view of the experimental set-up

by using two pressure transmitters (Setra C206, 0.13% of full scales that are 0-25 and 0-50 PSIG respectively). They are mounted to the valves placed at the inlet and outlet of the test unit and pressure values are recorded by the data acquisition unit. Validation and calibration of pressure transducers are carried out by measuring static water pressure for different heights. Pressure drop and convective heat transfer experiments are performed simultaneously. Measurements are repeated at least two times and mean value is reported if the results are consistent with each other.

2.4. Data Reduction

Thermophysical properties such as density and specific heat change when solid particles are added into a fluid. The density (ρ) and specific heat (c_p) of the nanofluid

can be defined based on basic mixture theory as

$$\rho_{nf} = \frac{\rho_{np}\rho_{bf}}{(1 - \phi)\rho_{np} + \phi\rho_{bf}} \quad (2.1)$$

$$c_{p,nf} = \phi c_{p,np} + (1 - \phi)c_{p,bf} \quad (2.2)$$

Here, ϕ represents particle mass fraction [%], and the subscripts nf , bf and np in the equations are the abbreviation of the words nanofluid, base fluid and nanoparticle, respectively.

Pressure transducers are mounted to the inlet and outlet of the test section to measure the pressure drop (ΔP) along the system. For laminar flow, pressure drop measurements are validated using Hagen-Poiseuille equation.

$$\Delta P = P_1 - P_2 = \frac{32\mu u_m L}{D^2} \quad (2.3)$$

where P_1 and P_2 are the fluid pressures at the inlet and outlet of the test section. Also, D , L , u_m and μ represent tube diameter (m), tube length (m), mean fluid velocity (m/s) and dynamic viscosity (Pa), respectively.

Then, Darcy-Weisbach equation is used to calculate the friction factor using ΔP .

$$f = \frac{\Delta P(D/L)}{\frac{1}{2}\rho u_m^2} \quad (2.4)$$

Well-known Poiseuille correlation (Equation 2.5) is used to validate the friction factor under laminar flow. Blasius (Equation 2.7) and Petukhov [68] (Equation 2.8) correlations are used for comparing experimental results beyond laminar region.

$$f = \frac{64}{Re_D} \quad (2.5)$$

$$Re_D = \frac{\rho u_m D}{\mu} \quad (2.6)$$

with Re_D is dimensionless Reynolds number.

$$f = 0.3164 Re_D^{0.25} \quad (2.7)$$

$$f = (1.82 \log(Re_D) - 1.64)^{-2} \quad (2.8)$$

Convective heat transfer measurements are first carried out by using DI water in the test system, then for the graphene-water nanofluids prepared with the mass fractions of 0.025%, 0.1% and 0.2%. The insulation quality of the test setup is determined by comparing the power supplied to the heater (q_{in}) with the heat transferred to system from heater (q_f). While q_{in} is 400 W in this study, q_f is calculated as follows

$$q_f = \dot{m} c_p (T_{m,o} - T_{m,i}) \quad (2.9)$$

where \dot{m} is the mass flow rate (kg/s), $T_{m,o}$ and $T_{m,i}$ are the fluid outlet and inlet mean temperatures ($^{\circ}C$), respectively. $T_{m,i}$ is measured by submerging a thermocouple into the flow at the inlet of the test pipe, whereas $T_{m,o}$ is measured at the outlet of the test pipe in a similar manner.

Heat loss of the experimental system is obtained by using Equation 2.10 and is lower than 8%.

$$q_{loss} = \left(1 - \frac{q_f}{q_{in}}\right) \times 100 \quad (2.10)$$

Local convective heat transfer coefficient, h_x , is calculated from Newton's law of cooling;

$$h_x = \frac{q_f / (\pi DL)}{T_w(x) - T_m(x)} \quad (2.11)$$

Here; $T_w(x)$ and $T_m(x)$ represents local wall and mean fluid temperatures ($^{\circ}C$) at axial position x , respectively. The mean temperature at a position x can be defined as;

$$T_m(x) = T_{m,i} + \frac{(q_f/L)x}{\dot{m}c_p} \quad (2.12)$$

where q_f is the heat transferred to system (W) and x is axial distance from the heated part of the test section (m).

Local Nusselt number, Nu_x , can be determined after calculating the local heat transfer coefficient.

$$Nu_x = \frac{h_x D}{k} \quad (2.13)$$

where k is thermal conductivity (W/m.K).

There are many empirical correlations in the literature to predict the local Nusselt number under laminar flow conditions. The expression developed by Shah and London [69] is used to validate the test setup for laminar flow in this study.

$$Nu_x = \begin{cases} 1.302(x^*)^{-1/3} - 1 & , x^* \leq 0.0005 \\ 1.302(x^*)^{-1/3} - 0.5 & , 0.0005 \leq x^* \leq 0.0015 \\ 4.364 + 0.263(x^*)^{-0.506} \exp(-41x^*) & , x^* > 0.0015 \end{cases} \quad (2.14)$$

where $x^* = (x/D)/(Re_D Pr)$ and represents dimensionless axial distance, and

$$Pr = \frac{\mu c_p}{k} \quad (2.15)$$

with Pr is dimensionless Prandtl number.

A wide flow range from laminar to turbulent flow is investigated in this study. In addition to laminar flow side, it is necessary to represent the equations used for transition and turbulent flow. Due to the instabilities in these regions, mean values of the heat transfer coefficient and Nusselt number are used instead of the local values. The mean heat transfer coefficient, \bar{h}_D , for the entire test unit is defined as;

$$\bar{h}_D = \frac{q_f / (\pi DL)}{\bar{T}_w - \bar{T}_f} \quad (2.16)$$

Here, \bar{T}_w is average temperature of the thermocouples mounted on the test unit and \bar{T}_f is average of the inlet and outlet temperatures. The mean Nusselt number is defined based on mean heat transfer coefficient accordingly.

$$\overline{Nu}_D = \frac{\bar{h}_D D}{k} \quad (2.17)$$

Mean Nusselt number is calculated by Gnielinski correlation for laminar flow (Equation 2.18) and validation study is done for DI water [70].

$$\overline{Nu}_D = \left[\overline{Nu}_{D,1}^3 + 0.6^3 + (\overline{Nu}_{D,2} - 0.6)^3 + \overline{Nu}_{D,3}^3 \right]^{1/3} \quad (2.18)$$

with the expressions as follows

$$\overline{Nu}_{D,1} = 4.354, \quad (2.19)$$

$$\overline{Nu}_{D,2} = 1.953 \sqrt[3]{Re_D Pr (D/L)} \quad (2.20)$$

$$\overline{Nu}_{D,3} = 0.924 \sqrt[3]{Pr} \sqrt{Re_D (D/L)} \quad (2.21)$$

For turbulent flow, Gnielinski correlation (Equation 2.22) is used to validate the mean Nusselt number of water [71].

$$\overline{Nu}_D = \frac{(f/8)(Re_D - 1000)(Pr)}{1 + 12.7\sqrt{f/8}(Pr^{2/3} - 1)} \quad (2.22)$$

where $2300 \leq Re_D \leq 10^6$ and $0.5 < Pr < 2000$, the friction factor, f , is estimated by using Petukhov equation (2.8)

2.4.1. Uncertainty Analysis

Uncertainty analysis of local heat transfer coefficient, Nusselt number and friction factor is carried out [72]. Uncertainties in flow rate, temperature, thermal conductivity and heat flux measurements cause an uncertainty in the heat transfer coefficient and Nusselt number. In the calculations, the accuracy of the measuring devices given above is used.

$$\sigma_{h_x} = \left[\left(\frac{\partial h_x}{\partial \dot{m}} \sigma_{\dot{m}} \right)^2 + \left(\frac{\partial h_x}{\partial T_w} \sigma_T \right)^2 + \left(\frac{\partial h_x}{\partial T_{m,i}} \sigma_T \right)^2 + \left(\frac{\partial h_x}{\partial q''} \sigma_{q''} \right)^2 \right]^{1/2} \quad (2.23)$$

The uncertainty of the heat flux, $\sigma_{q''}$, is calculated based on Equations 2.24 and 2.25 as;

$$q'' = \frac{\dot{m}c_p}{\pi D_h L} (T_{m,o} - T_{m,i}) \quad (2.24)$$

$$\sigma_{q''} = \left[\left(\frac{\partial q''}{\partial \dot{m}} \sigma_{\dot{m}} \right)^2 + \left(\frac{\partial q''}{\partial T_{m,o}} \sigma_T \right)^2 + \left(\frac{\partial q''}{\partial T_{m,i}} \sigma_T \right)^2 \right]^{1/2} \quad (2.25)$$

Then, the uncertainty of the Nusselt number is defined by the following equation.

$$\sigma_{Nu_x} = \left[\left(\frac{\partial Nu_x}{\partial \dot{m}} \sigma_{\dot{m}} \right)^2 + \left(\frac{\partial Nu_x}{\partial T_w} \sigma_T \right)^2 + \left(\frac{\partial Nu_x}{\partial T_{m,i}} \sigma_T \right)^2 + \left(\frac{\partial Nu_x}{\partial q''} \sigma_{q''} \right)^2 + \left(\frac{\partial Nu_x}{\partial k} \sigma_k \right)^2 \right]^{1/2} \quad (2.26)$$

In the Figure 2.8, the experimental uncertainties for the h_x and Nu_x under laminar flow are shown to be 8% and 9%, respectively. Beyond the laminar region, the uncertainties for the \bar{h}_D and \bar{Nu}_D are calculated similarly and increase up to 10% and 11% respectively.

In addition to heat transfer, the uncertainty calculations for the pressure drop and friction factor are performed by Equations 2.27 and 2.28. Results show that, the

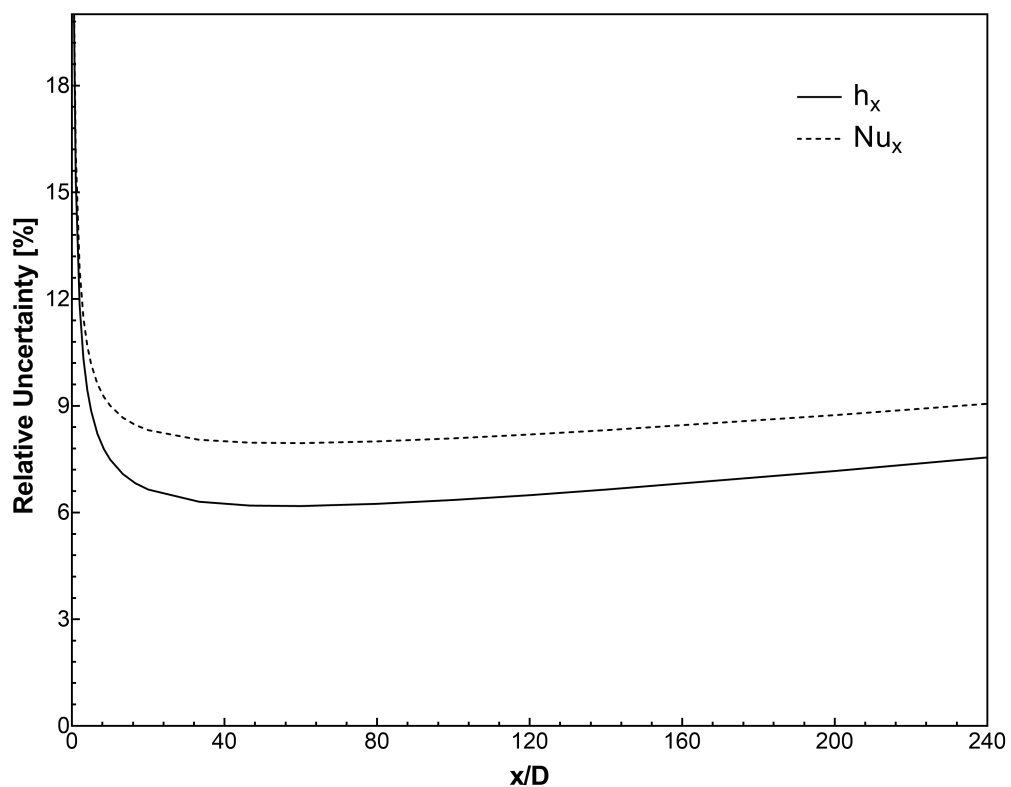


Figure 2.8. Relative uncertainty of h_x and Nu_x along the test tube

uncertainty of the pressure drop measurements for the range from laminar to turbulent flow is below 2%, whereas friction factor is below 5%.

$$\sigma_{\Delta P} = \left[\left(\frac{\partial \Delta P}{\partial P_1} \sigma_{P_1} \right)^2 + \left(\frac{\partial \Delta P}{\partial P_2} \sigma_{P_2} \right)^2 \right]^{1/2} \quad (2.27)$$

$$\sigma_f = \left[\left(\frac{\partial f}{\partial \Delta P} \sigma_{\Delta P} \right)^2 + \left(\frac{\partial f}{\partial u_m} \sigma_{u_m} \right)^2 \right]^{1/2} \quad (2.28)$$

3. RESULTS AND DISCUSSION

3.1. Morphological Characterization

ESEM images are used for characterization of the dry graphene nanoparticles and to evaluate their compliance with the manufacturer's datasheet. While the particle sizes observed in Figure 3.1 are consistent with the manufacturer's specifications, some agglomerations up to $5\mu\text{m}$ among the graphene nanoparticles are observed. The methodology explained before is applied for the production of the graphene-water nanofluid. After the dry graphene nanoparticles are dispersed into water, ultrasonic mixing is applied to break these aggregates.

The STEM images of the dried nanofluids are presented in Figure 3.2, where it can be observed that graphene flakes form loosely percolating structures with size of these structures in the order of few micrometers. In addition to the STEM imaging, DLS measurements are carried out. As two dimensional materials such as graphene are approximated as spherical particles in DLS, intensity based size distribution are reported in terms of diameters (d.nm) as presented in Figure 3.3. It can be observed that the majority of the particles are around 600 d.nm, which is consistent with STEM images. Besides, the z-average in DLS measurements that represents the intensity

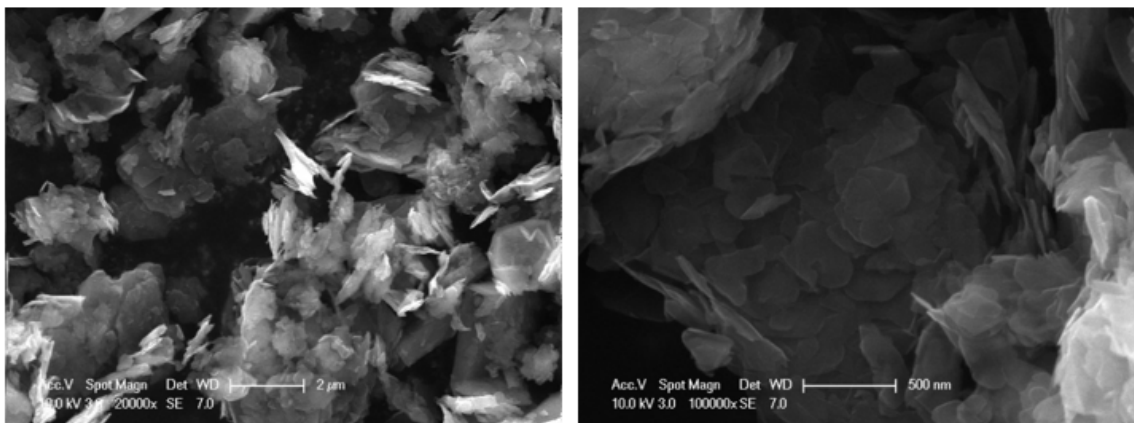


Figure 3.1. ESEM images of dry graphene nanoparticles

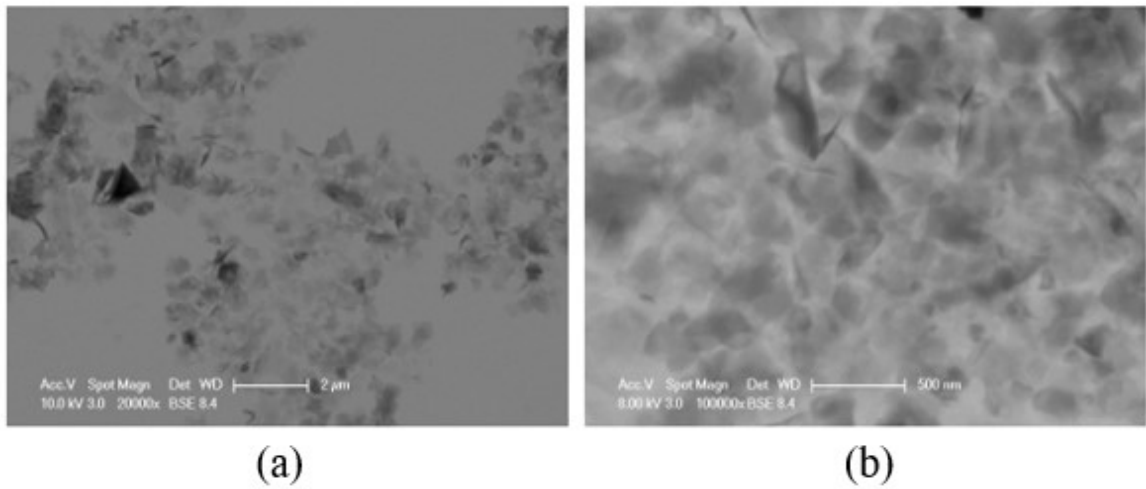


Figure 3.2. STEM images of graphene-water nanofluids for different mass concentrations (a) 1%, (b) 0.5% with the scales 2 μm and 500 nm respectively

based cumulative average particle size is found to be 443 d.nm. Therefore, it can be concluded that the applied ultrasonication time is sufficient for preventing the possible aggregates in the nanofluid.

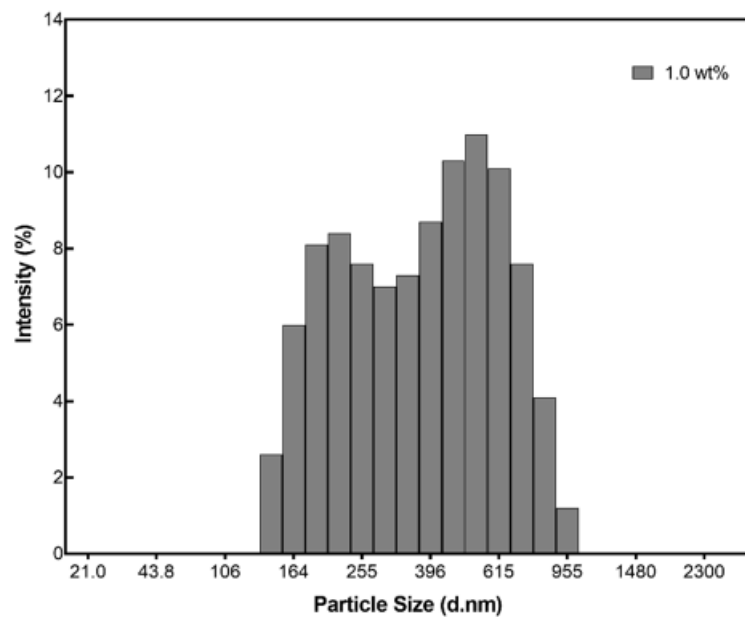


Figure 3.3. Particle size distribution of graphene-water nanofluid by DLS measurements

3.2. Material Characterization

Raman spectrum of the graphene nano-flakes is shown in Figure 3.4. The range of the spectrum is $100\text{-}2000\text{ cm}^{-1}$ and it can be observed that the G and D peaks appear at 1572 cm^{-1} and 1341 cm^{-1} , respectively. The location of the G peak indicates that the graphene nano-flakes are comprised of few layers. The intensity ratio of the D and G peaks (I_D/I_G) equals to 0.77, and this relatively high ratio suggests that some defects might have occurred during the exfoliation of graphene nanosheets from the graphite. Nevertheless, the quality of the graphene sheets used in the experiments appears to be acceptable comparing the intensity ratio to those reported in the literature [65].

3.3. Stability Characterization

Stability assessment of the produced nanofluids is critical as stability is considered to be one of the major challenges for industrialization of nanofluids. Zeta potential measurements are used to assess the stability by diluting the nanofluid samples to

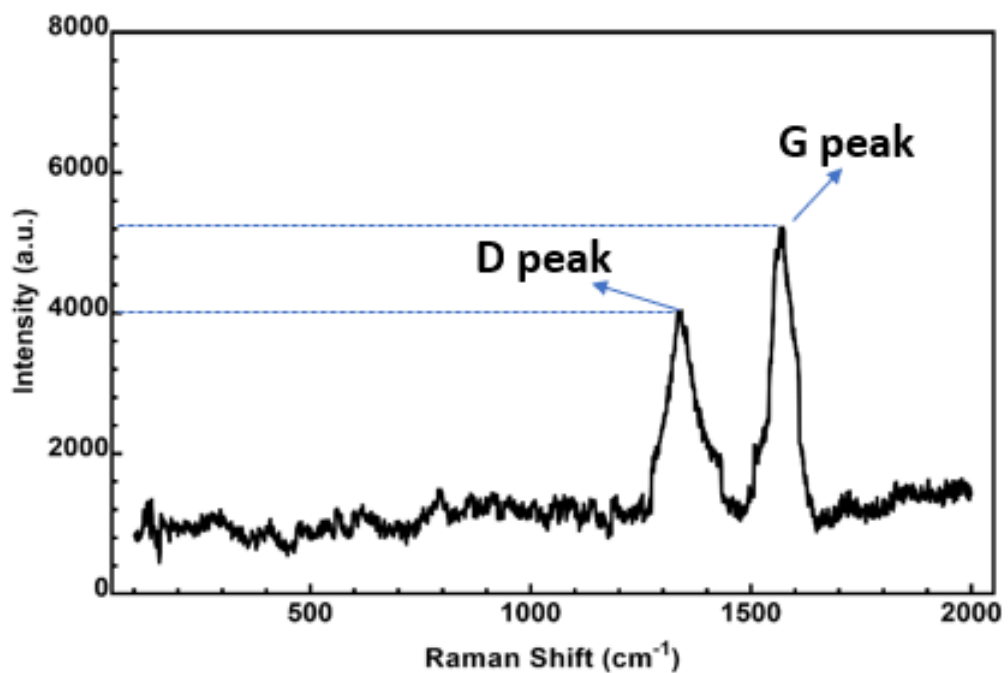


Figure 3.4. Raman spectrum of the graphene nanosheets

0.01% particle mass fraction. A study is carried out for determining the nanoparticle-surfactant ratio required for achieving stable suspensions. The results of the study are presented in Table 3.1 for 1% particle mass fraction, where it can be seen that nanoparticle-surfactant ratio of 1-1 provides the highest stability. Therefore, this ratio is used for preparing all nanofluids in this study. The measured zeta potential for 1-1 ratio is -39.2 mV, indicating that the suspension is stable. Moreover, long-term stability is assessed by performing zeta potential measurements 20 and 30 days after the production of the samples, and zeta potential is measured as -36.5 mV after 20 days and -32.8 mV after 30 days. These values resemble acceptable long term stability considering the literature [55, 73].

Table 3.1. Zeta potential values with respect to different nanoparticle-PVP ratios

Nanoparticle-PVP Ratio	Zeta Potential (mV)
1-0.2	-29.6 \pm 2%
1-0.5	-34.8 \pm 2%
1-1	-39.2 \pm 2%
1-1.5	-38.5 \pm 2%

3.4. Rheological Characterization

Rheological behavior of the prepared graphene-water nanofluids is investigated next. The viscosity measurements are validated by measuring the dynamic viscosity of DI water at different temperatures. Dynamic viscosities of five different samples with particle mass fractions from 0.1 to 2% are then measured. The measurements are performed by increasing the shear rates from 375 to 1875 sec^{-1} at 25°C and the average of the measured viscosity values is reported as the viscosity of each concentration. The relative viscosity (μ_{nf} / μ_{bf}) of the nanofluid is presented based on measured viscosity of water. The relative and absolute viscosity with respect to particle mass fraction at 25°C

is shown in Figure 3.5. The maximum relative viscosity increase is found to be 45% for 2%. The slope of the relative viscosity line changes significantly after 1%, where percolation networks become more effective. Zheng *et al.* [74] reported that the percolation threshold of the graphene nanofluids is around 1% particle fraction that is in agreement with the results presented. The temperature dependence of the viscosity is also investigated for a temperature range varying from 25 to 60 °C. The measured change of absolute and relative viscosity with temperature is presented in Figures 3.6 and 3.7, respectively. It can be observed that the absolute viscosity of the nanofluid decreases with the increased temperature; whereas, relative viscosity remains almost constant. This indicates that the temperature dependence of the graphene-water nanofluids is due to the temperature dependence of base fluid's viscosity, and changing temperature does not have a significant effect on the mechanisms affecting the viscosity of the nanofluid. The change in thermo-physical properties due to Brownian motion depends on temperature as discussed by Prasher *et al.* [75]; whereas, the percolation effect does not vary with temperature as reported by Gupta *et al.* [38]. Considering these, it can

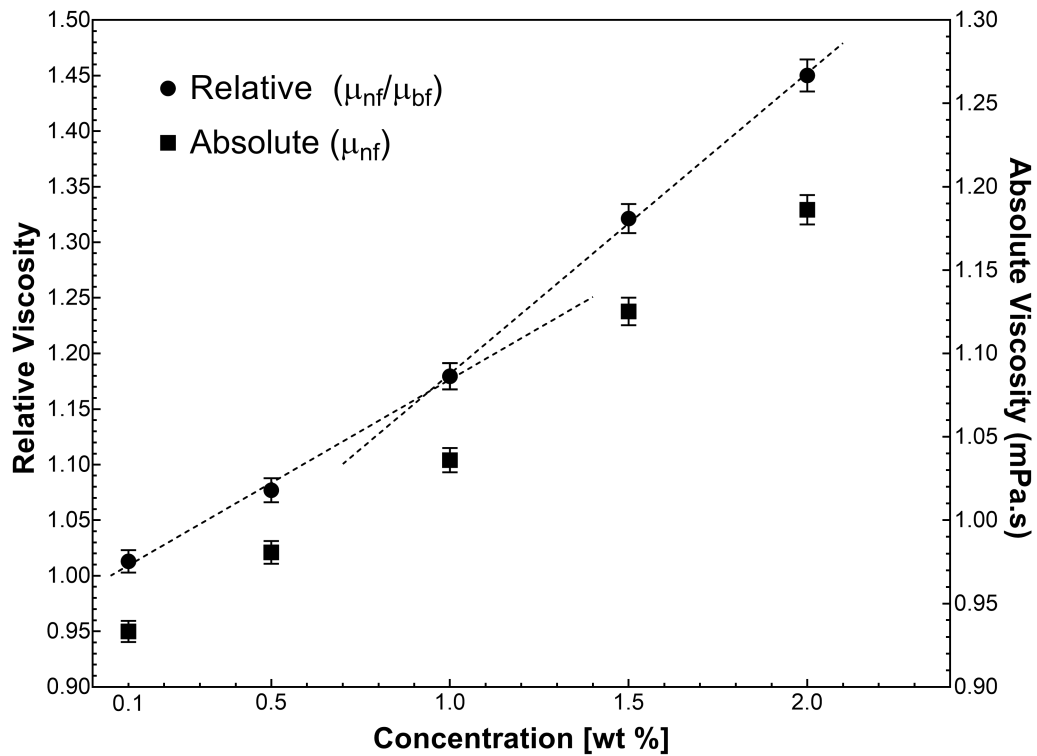


Figure 3.5. Change of the viscosity with respect to the concentration at 25°C

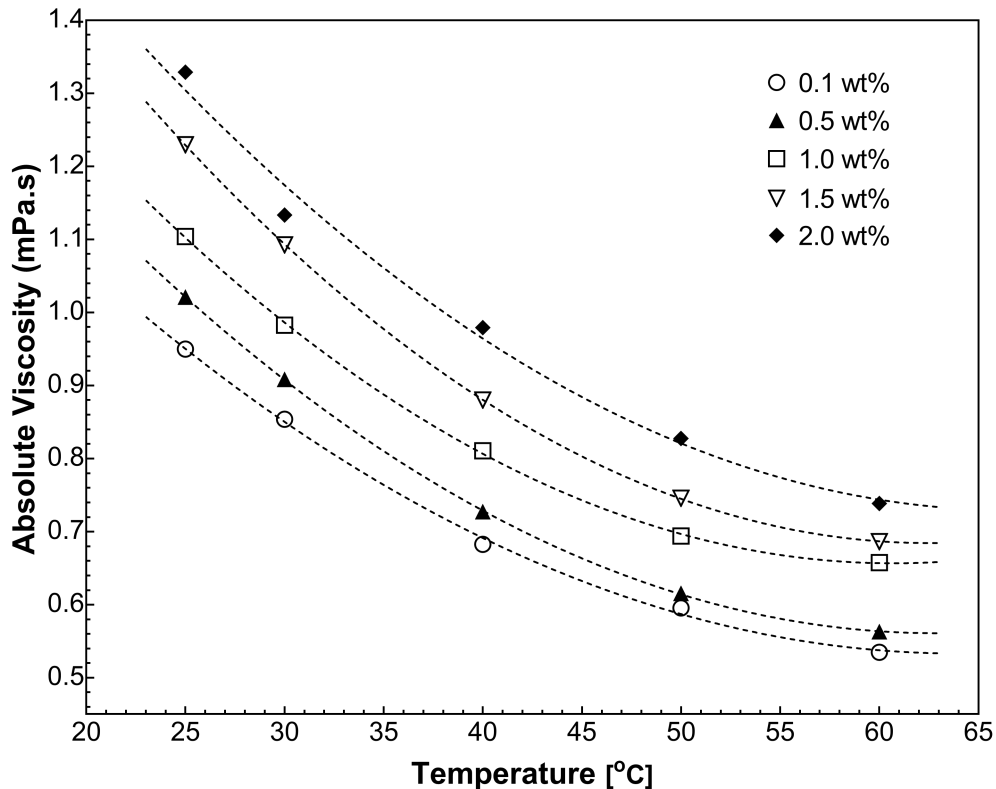


Figure 3.6. Absolute viscosity change with temperature

be concluded that percolation effects are more dominant than the effects of Brownian motion for the graphene-water nanofluids investigated.

The viscosity of the nanofluids at different shear rates is analyzed for identifying rheological characteristics. The relative viscosity change with respect to different shear rates at 25°C is presented in Figure 3.8, where relative viscosity is measured by gradually increasing the shear rates from 375 to 1875 sec^{-1} . While Newtonian behavior is observed for nanofluids with relatively lower particle concentrations ($\phi < 0.5\%$); shear thinning behavior is observed for particle mass fractions above 0.5%. The non-Newtonian behavior becomes more pronounced for the higher particle concentrations. Wang *et al.* [76] studied graphene oxide-EG nanofluids with 0.5 to 2% particle mass fraction and observed similar behavior at higher fractions. They explained this change of the rheological characteristic by percolation networks. The viscosity decreases with increasing shear rates; the relative viscosity of the 1.5% sample declines 4.8% as shear rate increases from 375 to 1175 sec^{-1} , whereas the decline is 1% as shear rate increases

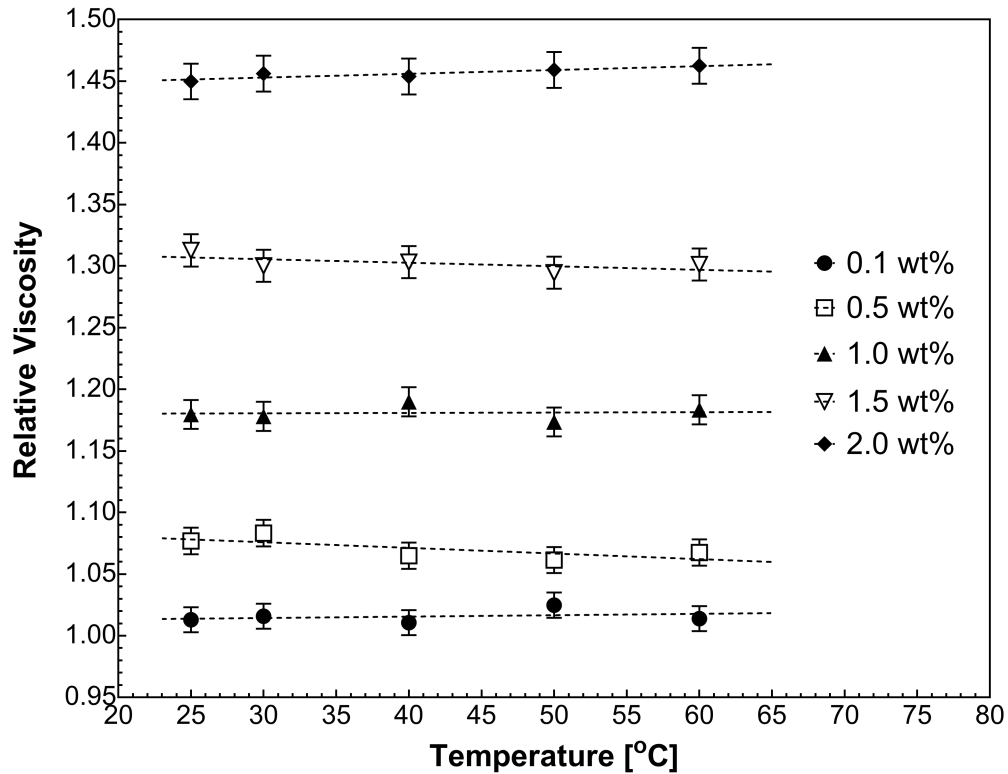


Figure 3.7. Relative viscosity change with temperature

from 1175 to 1875 sec^{-1} . It appears that relatively lower shear rates are enough to disintegrate the loosely percolating structures observed in Figure 3.2 leading to a decrease in viscosity, and further increase in shear rates does not have a further significant effect resulting in a milder decrease in viscosity. Similar observations are also valid for nanofluids with 1 and 2% around the same shear rates. Moreover, the relative viscosity values at higher shear rates presented in Figure 3.8 is in agreement with the predictions of Batchelor [77] correlation that considers Brownian motion effects. Therefore, it can be concluded that at lower shear rates the nanofluid is more viscous due to the presence of both percolation and Brownian motion induced mechanisms, whereas, the percolating structures disintegrate with increasing shear rates and viscosity increase is due to Brownian motion induced effects.

Hysteresis is investigated next, by measuring viscosity by first gradually increasing the shear rate from 375 to 1875 sec^{-1} , and then reducing it gradually back to 375 sec^{-1} at different temperatures. Figure 3.9 shows the change in the absolute viscosity

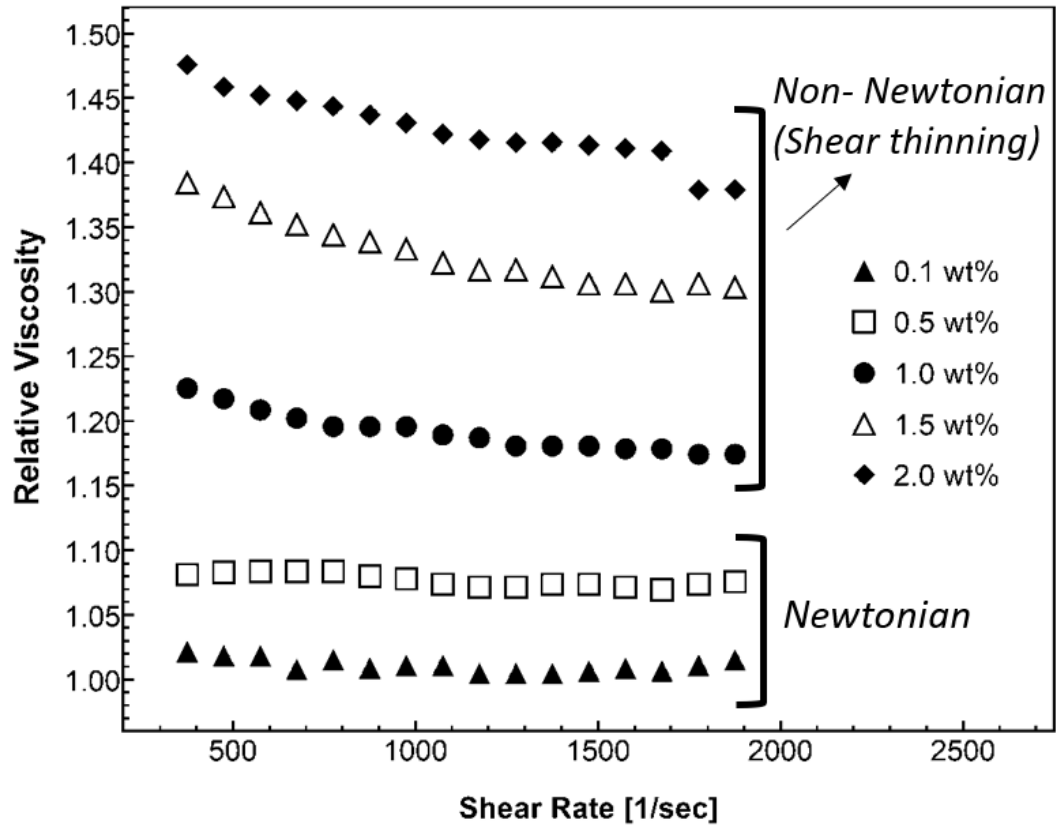
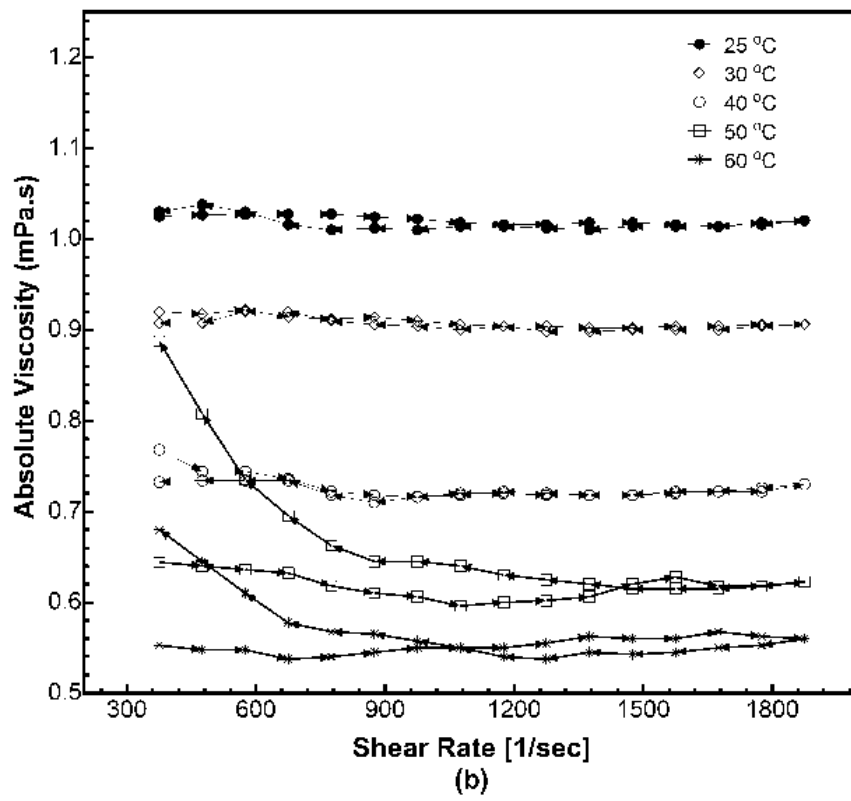
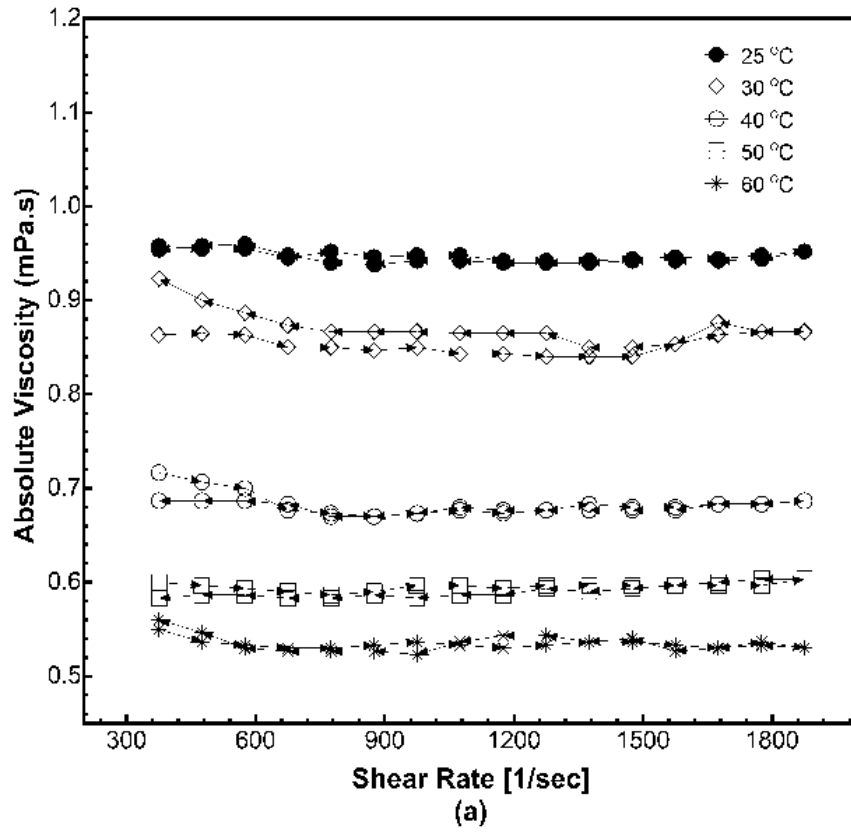
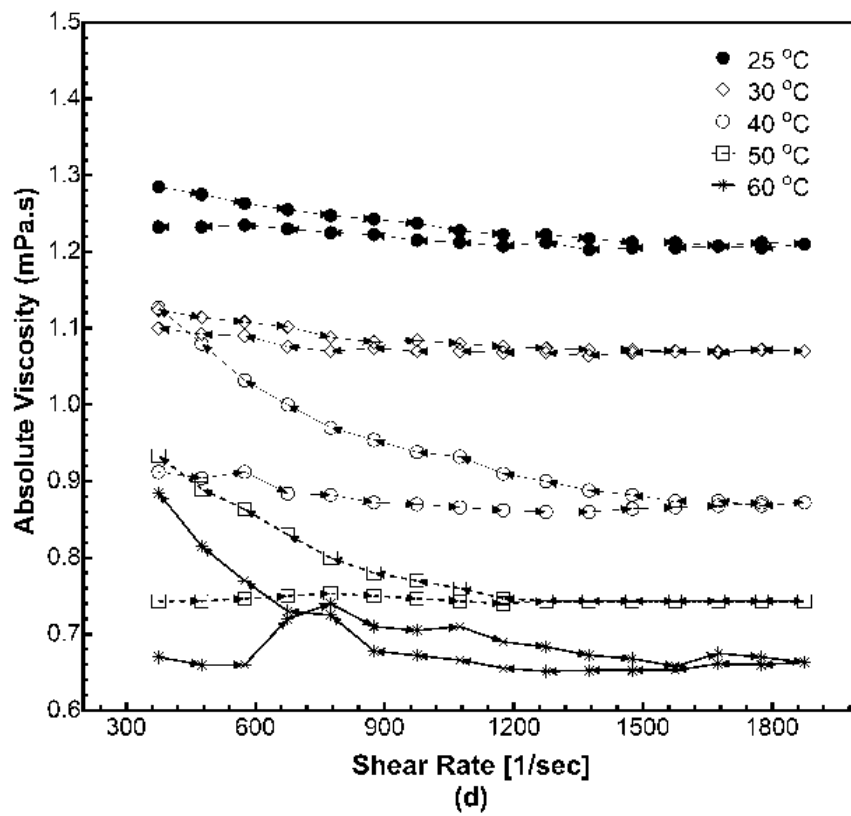
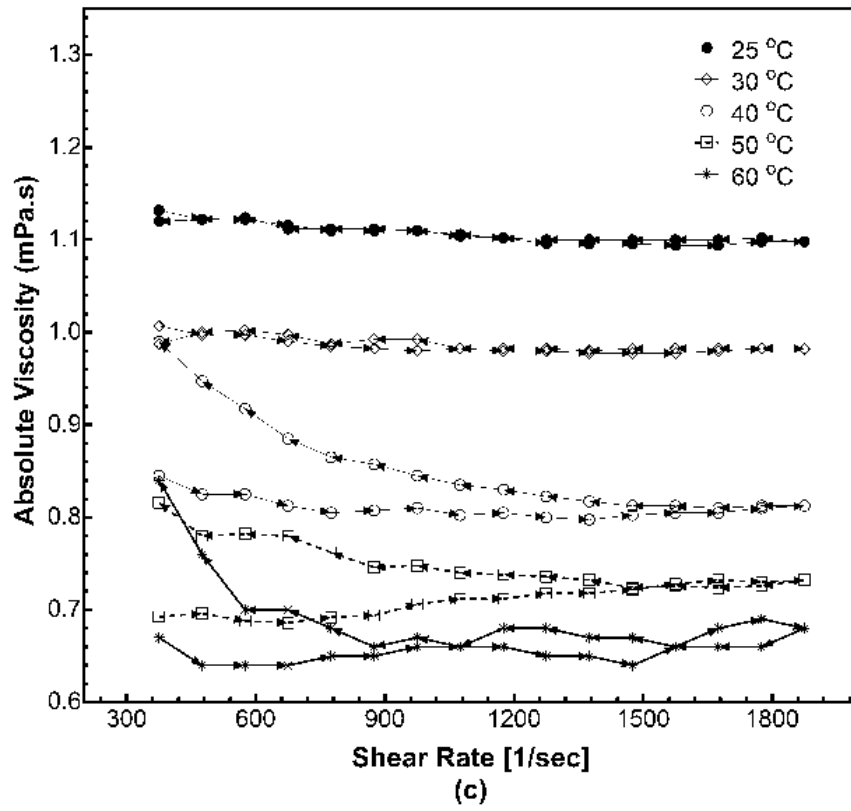


Figure 3.8. Relative viscosity variation with respect to the different shear rates at 25°C

of graphene-water nanofluids with different concentrations, at different temperatures, with changing shear rates, both increasing and decreasing. The viscosity is approximately same for increasing or decreasing shear rates for 0.1% particle mass fraction graphene-water nanofluid. Hysteresis in the viscosity can be observed at or above 50 °C for 0.5% particle mass fraction. Here the viscosity does not change with increasing shear rate; whereas, it increases as the shear rate decreases beyond 900 sec^{-1} , exhibiting a shear thinning behavior. Similar behavior can be observed at or above 40 °C for 1% and 1.5% particle mass fractions, with viscosity increasing once shear rate decreases from 1600 sec^{-1} for 40 °C. The 2% particle mass fraction nanofluid exhibits shear thinning behavior for both increasing and decreasing shear rates. However, the shear thinning behavior is more pronounced for decreasing shear rates.





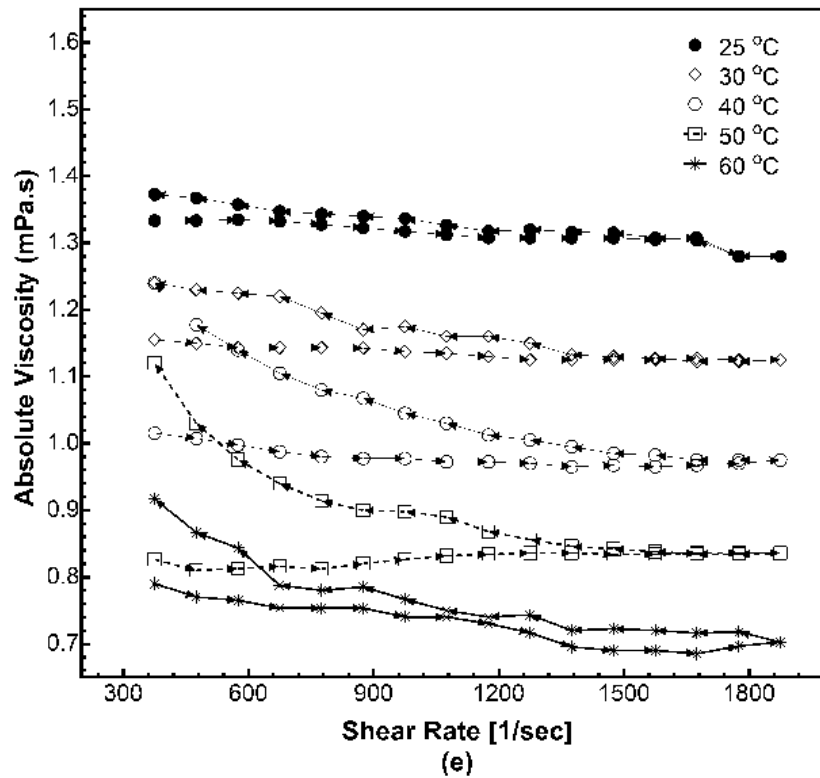


Figure 3.9. Hysteresis analysis of the graphene/water nanofluids for different particle mass fractions (a) 0.1%, (b) 0.5%, (c) 1.0%, (d) 1.5%, (e) 2.0% (lines with \rightarrow indicates the measurements increasing shear rate cases, and lines with \leftarrow indicates the decreasing shear rates)

3.5. Thermal Characterization

Thermal conductivity measurements are performed at 25 °C for all the samples with different particle mass fractions. Thermal conductivity of water and EG are measured for validation prior to the thermal conductivity measurement of nanofluids. The change of relative thermal conductivity (k_{nf}/k_{bf}) of graphene-water nanofluids with particle mass fraction is presented in Figure 3.10. It can be observed that the thermal conductivity enhancement with respect to DI water monotonically increases from 22% for 0.1% to 96% for 2%. It appears that the conductivity increase is relatively gradual until 1% particle mass fraction is reached, where thermal conductivity increase is about 40%. This concentration appears to be the percolation limit, and thermal conductivity

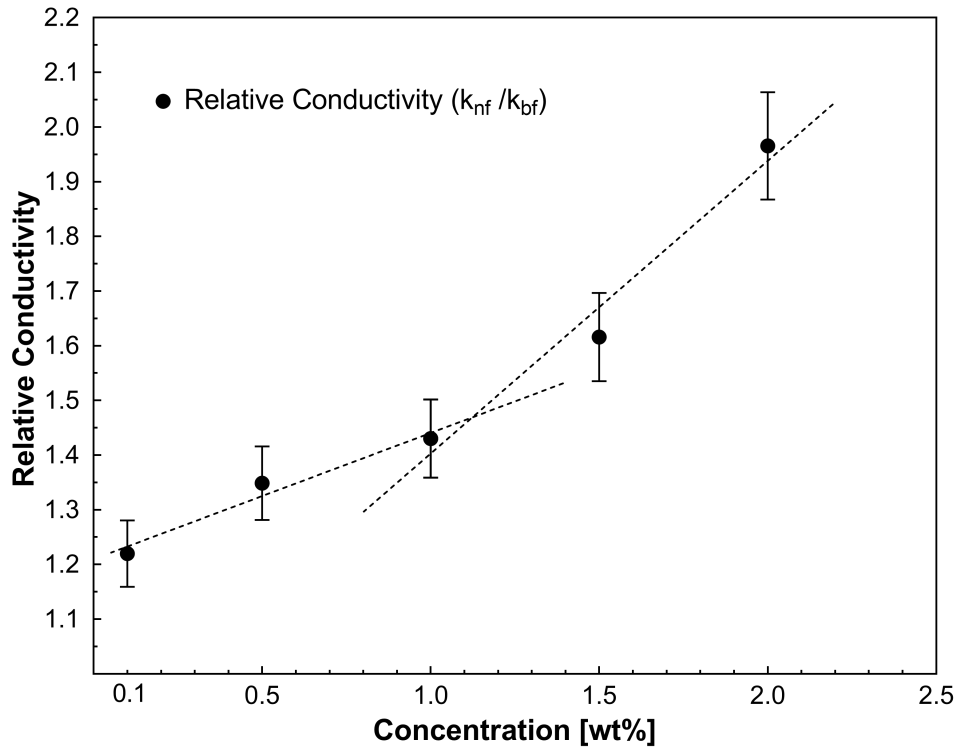


Figure 3.10. Relative thermal conductivity of graphene-water nanofluids at 25°C

increase accelerates exceeding this concentration due to increased effectiveness of the percolation networks.

3.6. Thermophysical Property Comparison with Literature

The results presented are in the agreement with the literature as shown in Table 3.2, where summary of results of the current study is presented together with data from literature.

3.7. Forced Convection in Nanofluids

3.7.1. Pressure Drop and Friction Factor

Pressure drop (ΔP) and friction factor (f) of graphene-water nanofluids with 0.025, 0.1 and 0.2% particle mass fractions are investigated for a Reynolds number

Table 3.2. Thermo-physical property comparison of different graphene/surfactant solutions in the literature

Author	Nanofluid / Surfactant	Concentration	Thermal Conductivity Enhancement	Viscosity Increase
Current Study	GnP-DW / PVP	0.1-2.0 wt%	Up to 96%	Up to 45%/
[78]	GnP-EG / DOC GnP-DW / DOC	0.001-0.5 vol%	21% 16%	-
[43]	GnP-DW / CTAB GnP-DW / GA GnP-DW / SDBS GnP-DW / SDS	0.1 wt%	5.8% 10.8% 8.3% 1.4%	6.9% 116.9% 7.4% 4.5%
[79]	(ND)Graphene- DW / Triton X-100	0.01-0.06 wt%	Up to 37%	-
[80]	GnP-DW/SDBS	0.05-0.15 vol%	Up to 49%	Up to 47.1%
[81]	GnP-DW / P123	0.1 wt%	Up to 24.4%	Up to 47%
[82]	GnP-DO / OA	0.05-0.5 wt%	Up to 68%	-

range of 1400 to 4000. A validation study is carried out with DI water, and the friction factor results are compared with Poiseuille (Equation 2.5), Blasius (Equation 2.7) and Petukhov (Equation 2.8) correlations. In the laminar flow, experimental results of friction factor and Poiseuille correlation are in the agreement for DI water. In turbulent region, friction factor measurements for DI water exceed the predictions by Blasius correlation, but they are in close agreement with predictions by the Petukhov correlation.

Measured pressure drop for a range of 1400 to 4000 Reynolds number is shown in Figure 3.11. It increases with increasing particle concentration and flow rate. Ratio of

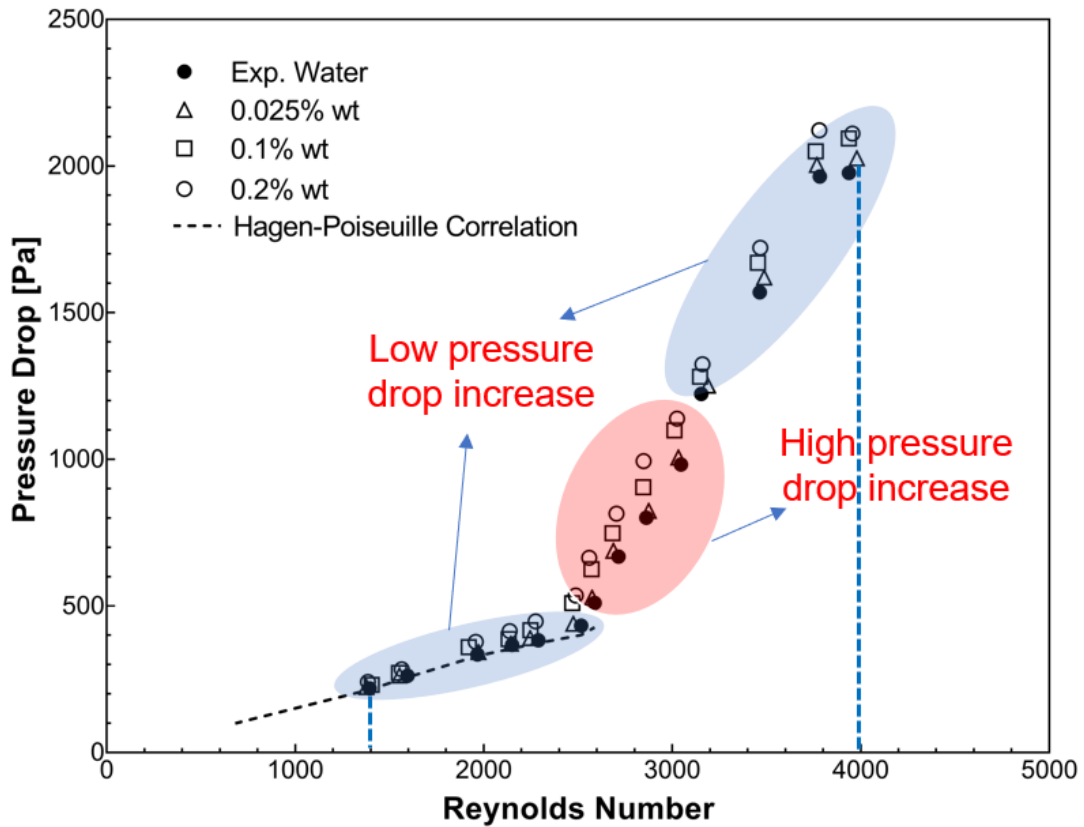


Figure 3.11. Pressure drop change for different concentrations and flow rates

the pressure drop of the nanofluids to that of water in the transition zone is significantly higher than other regions. Chaotic fluctuations after smooth laminar flow might cause a high loss here. Even though measured maximum pressure drop for the nanofluids is 30% higher than water in the transition regime, the increase in the pressure drop measurements are less than 10% for laminar and turbulent regimes. Therefore, working with the graphene nanofluids are used operation within the in transition regime should be avoided due to its high pressure drop.

Laminar, transition and turbulence regions of water and graphene-water nanofluids are seen clearly in Figure 3.12. In the laminar flow, friction factor decreases with increasing Reynolds number. The friction factor decline trends for water and graphene nanofluids are similar. The friction factor of DI water and nanofluid with 0.025% particle concentration is nearly identical through the laminar region, whereas it is higher

for the nanofluids with 0.1% and 0.2% at a given Reynolds number. For water and the nanofluid of 0.025% concentration, the increase in friction factor starts after around a Reynolds number of 2450 and continues up to $Re_D \approx 3150$, where laminar to turbulent transition takes place. It can be seen in Figure 3.12, the transition starts at smaller Reynolds numbers for nanofluids with higher particle concentrations as agreement with other studies [83–85]. The onset of laminar to transition flow and transition flow to turbulence are determined by linear and nonlinear regression to the measured friction factors, and listed in Table 3.3. Laminar to turbulence transition shifts to a lower Reynolds number by $\sim 4\%$ for 0.1% particle mass fraction and $\sim 7\%$ for 0.2% particle mass fraction while the early transition phenomenon is observed with an increase in the concentration. The slope of increasing the friction factor with respect to Reynolds number in the transition region is almost identical for water and all the nanofluids tested. Friction factor of DI water and the nanofluid with 0.025% mass concentration starts to decrease after $Re_D \approx 3150$ whereas the corresponding Reynolds number is

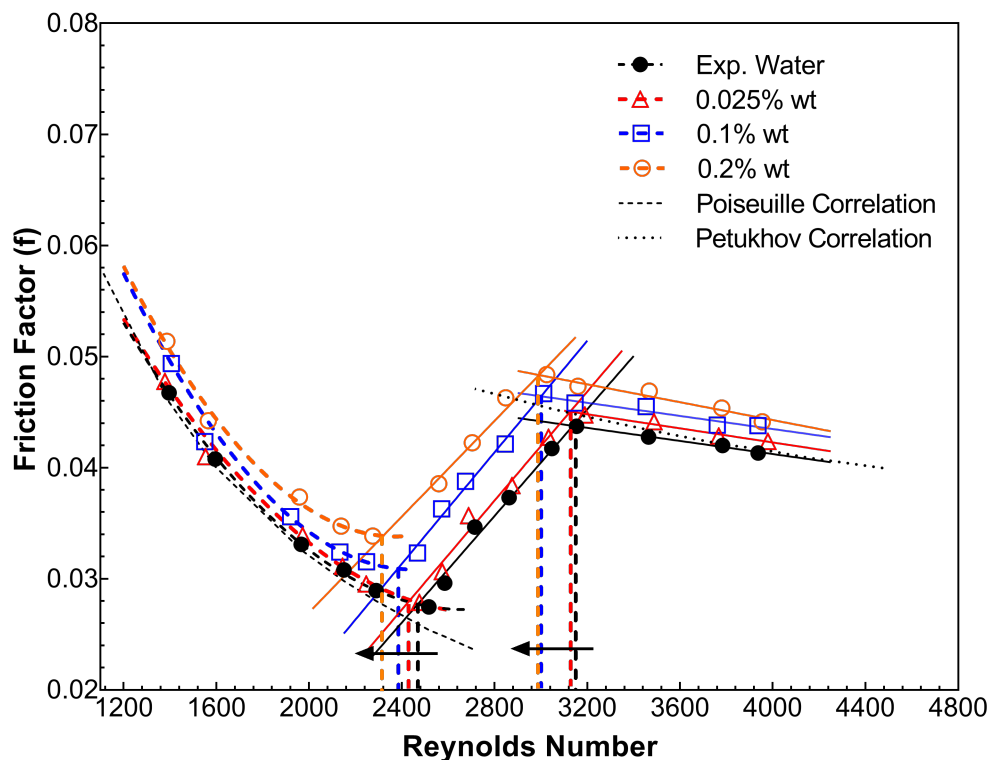


Figure 3.12. Friction factor change trends for laminar, transition and turbulent flow

Table 3.3. Approximate onset of the transition and turbulence regimes in terms of Reynolds number according to pressure drop measurement

Sample	Onset of Transition (Re_D)	Onset of Turbulence (Re_D)
Water	2475 ± 50	3150 ± 65
0.025% nf	2435 ± 50	3125 ± 65
0.1% nf	2385 ± 50	3010 ± 60
0.2% nf	2315 ± 45	2990 ± 60

about 3000 for 0.1% and 0.2% nanofluid. Hence, the transition takes place for the nanofluids of 0.1% and 0.2% is shorter than water and nanofluid with 0.025% particle mass concentration. One possible reason of the early transition is extra disturbance caused by the graphene nanoparticles in denser nanofluids [86]. Beyond $Re_D=3200$, friction factors for all samples decreases with increasing Reynolds number with similar trends and the flow in the pipe turns to fully turbulent.

3.7.2. Heat Transfer Coefficient and Nusselt Number

Convective heat transfer performance of the graphene-water nanofluids is investigated for nanofluids with 0.025, 0.1 and 0.2% particle mass fractions focusing on transition from laminar to turbulent flow. Validation studies are carried out for DI water before testing nanofluids, by comparing measurements with predictions of Shah and London [69] and Gnielinski [70] correlations for laminar flow, and Gnielinski correlation [71] for turbulent flow. The experimental measurements are in the agreement with predictions based on correlations as seen in Figures 3.13 and 3.14. It should be note that the laminar regime in this study has hydrodynamically developed and thermally developing characteristics, whereas the flow is fully developed in turbulence region.

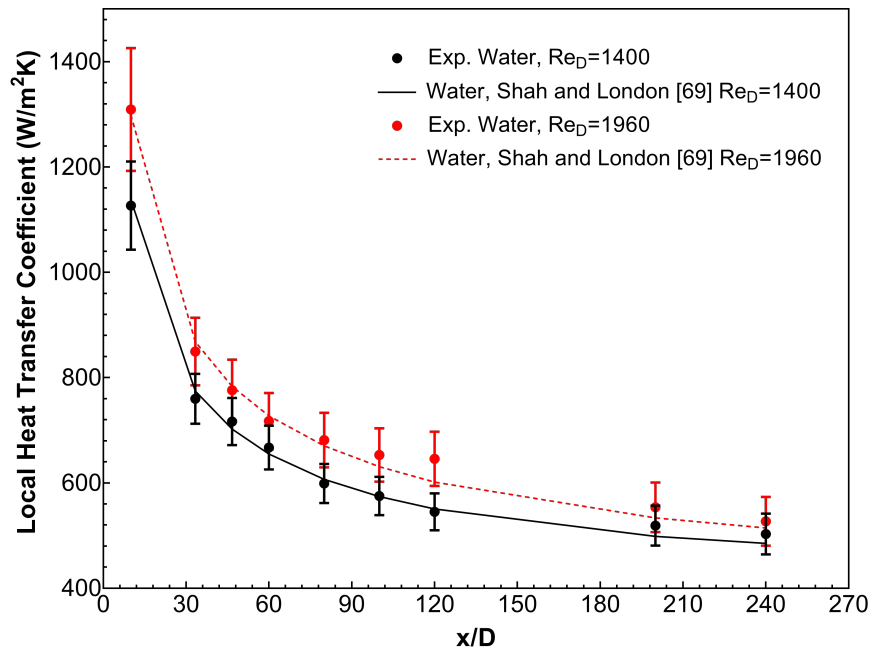


Figure 3.13. Comparison of local heat transfer coefficient measurements with Shah and London correlation [69] for DI water at $Re_D=1400$ and $Re_D=1960$

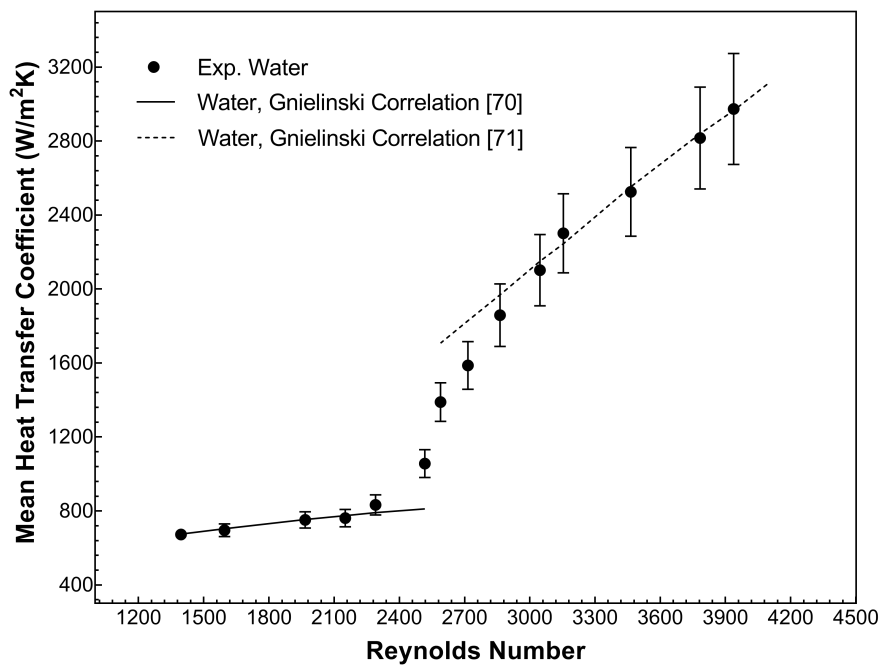


Figure 3.14. Comparison of mean heat transfer coefficient measurements with Gnielinski correlations [70, 71] for DI water

Experiments are carried out for a range of Reynolds numbers and with three different nanoparticle concentrations to investigate the flow rate and concentration effects on heat transfer in different flow regimes. For the laminar flow, local heat transfer coefficient of graphene-water nanofluids is measured in various flow rates and shown for $Re_D=1400$ and $1950 (\pm 50)$ in Figure 3.15. It is observed that local heat transfer coefficient, h_x , of both water and graphene nanofluids increase with flow rate, and particle concentration. Local heat transfer coefficient enhancement for the particle mass concentrations of 0.025, 0.1 and 0.2% at different axial locations and Reynolds numbers is shown in Table 3.4. Since increase in heat transfer coefficient is nearly same for given concentrations at $x/D=120$ and $x/D=240$, it can be argued that the flow is hydrodynamically fully developed after $x/D=120$, but it is still thermally developing. Also, local heat transfer coefficient enhancement depends on the concentration in laminar flow rather than flow rate considering the measurement precision. In order to better understand the effective heat transfer mechanisms under laminar flow, mean heat transfer

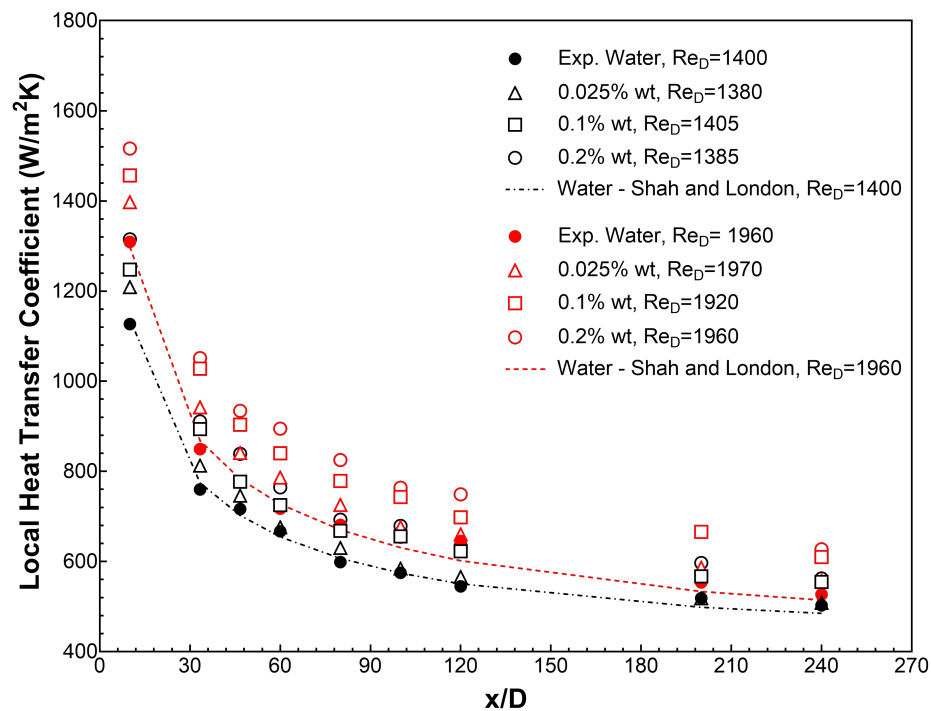


Figure 3.15. Local heat transfer coefficient of graphene-water nanofluids for 0.025, 0.1 and 0.2% mass concentration at $Re_D \approx 1400$ and $Re_D \approx 1950$

Table 3.4. Local heat transfer coefficient increase of graphene-water nanofluids for $Re_D \approx 1400$ and 1950 at $x/D = 120$ and $x/D = 240$

For $x/D=120$			
	0.025 wt%	0.01 wt%	0.2 wt%
$Re_D=1400$	3.6%	12.1%	15.4%
$Re_D=1950$	2.5%	8.1%	15.2%
For $x/D=240$			
	0.025 wt%	0.01 wt%	0.2 wt%
$Re_D=1400$	3%	11.2%	14.8%
$Re_D=1950$	3.6%	12.8%	17.4%

coefficient, \bar{h}_D , is also investigated at a Reynolds number of 1400 and 1950. Mean heat transfer coefficient enhancement for 0.025, 0.1 and 0.2% particle mass fraction is 7.3, 17.2 and 22.7% at $Re_D=1400$ and 7.2, 17.6 and 22.8% at $Re_D=1950$, respectively. Therefore, the enhancement in convective heat transfer coefficient is largely due to the enhancement in thermal conductivity for laminar flow (Figure 3.16). The effect of the thermal conduction on heat transfer can be seen more clearly in Figure 3.17. Similar with the local heat transfer coefficient enhancement, local Nusselt number values also do not change significantly in different concentrations, but change with different flow rates.

Heat transfer in laminar to turbulence transition is investigated next, by further increasing the Reynolds number from 1950 to 4000. Figure 3.18 illustrates the mean heat transfer coefficient, \bar{h}_D , change of graphene-water nanofluids with respect to Reynolds number. In addition, the mean heat transfer coefficient change trends for laminar, transition and turbulent flow regimes are shown in Figure 3.19. For laminar flow, mean heat transfer coefficients of all three nanofluids show parallel trends, slightly increasing with Reynolds numbers nearly from 1400 to 2200. But, the heat transfer behavior of water and graphene-water nanofluids begins to change beyond $Re_D \approx 2200$.

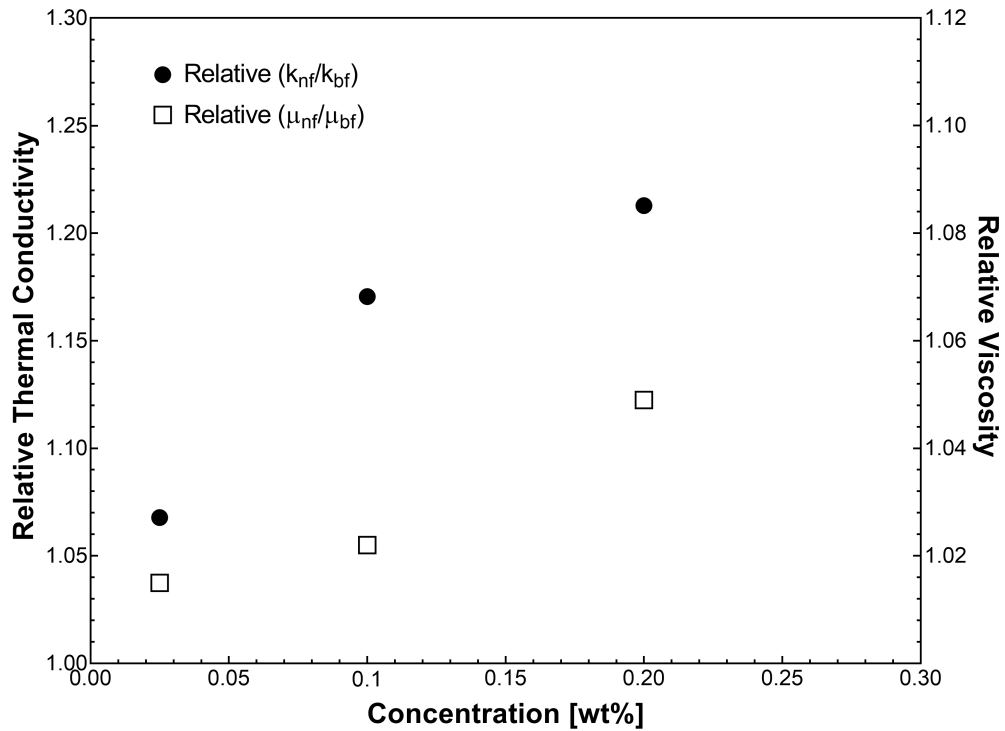


Figure 3.16. Relative thermal conductivity and viscosity of graphene-water nanofluids for 0.025, 0.1 and 0.2% mass concentration

The approximate onset of the laminar to turbulent transition and turbulent flow are listed in Table 3.5. Transition is observed at lower Reynolds numbers with increasing concentration as it is seen in Table 3.5. There is a dramatic increase in mean heat transfer coefficient of DI water at around a Reynolds number of 2450, and mean heat transfer coefficient converges to Gnielinski correlation (2.22) nearly at 3150 as it is consistent with the friction factor results (Table 3.3). Even though the transition takes place earlier than water and the observation is in the agreement with the studies in the literature [84,87,88], transition observed relying on the heat transfer measurements is at lower Reynolds numbers for tested nanofluids than those reported by relying on the friction factor measurements. The onset of the laminar to transition regime for the nanofluids with 0.025, 0.1 and 0.2% particle mass concentrations are around at a Reynolds number of 2370, 2250 and 2200 in the heat transfer measurements, whereas it is 2435, 2385 and 2315 in the friction factor measurements, respectively. It means that mean heat transfer coefficient for the graphene-water nanofluids begins to increase

Table 3.5. Approximate onset of the transition and turbulent flow regimes in terms of Reynolds number according to heat transfer measurements

Sample	Onset of Transition (Re_D)	Onset of Turbulence (Re_D)
Water	2440 ± 50	3160 ± 65
0.025% nf	2370 ± 50	3155 ± 65
0.1% nf	2250 ± 45	3020 ± 60
0.2% nf	2200 ± 45	2970 ± 60

significantly before transition flow which is determined in the friction factor measurements. On the other hand, the onset of the turbulent flow is almost same for heat

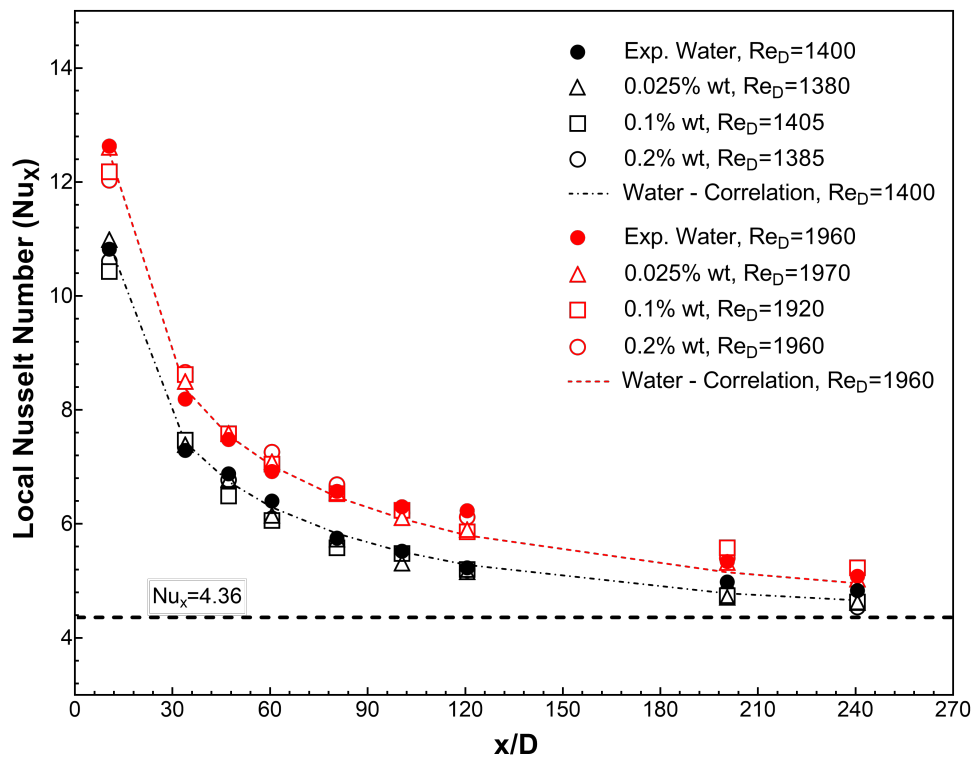


Figure 3.17. Local Nusselt number of graphene-water nanofluids for 0.025, 0.1 and 0.2% mass fraction

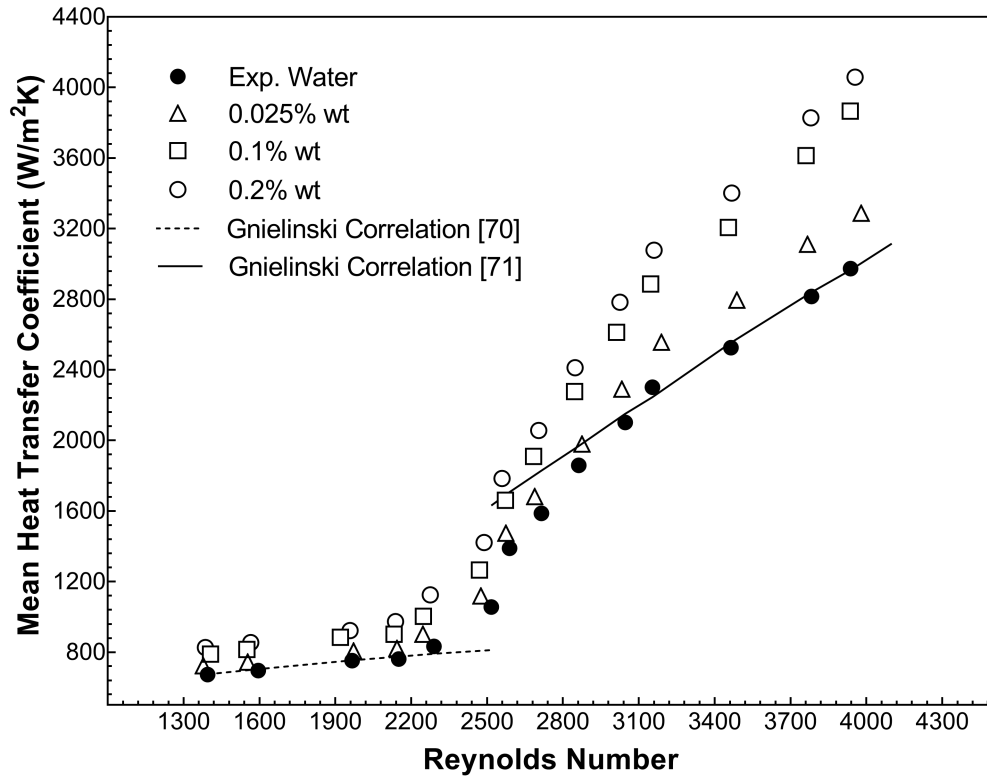


Figure 3.18. Mean heat transfer coefficient change of graphene-water nanofluids for 0.025, 0.1 and 0.2% mass concentration

transfer measurements as accordance with friction factor measurements. One reason of the early transition phenomenon is the addition of the solid particles into the base fluid. After graphene-water nanofluids are prepared by adding graphene nanoparticles into water, the nanoparticles disturb and fluctuate the flow during the circulation. Therefore, inertia forces become more effective with the introduced fluctuations at earlier. Moreover, the viscosity of the nanofluids is higher than the base fluid (Figure 3.16). This leads the nanofluid have lower Reynolds number than its base fluid at a given flow rate and the transition takes place earlier in terms of Reynolds number. The experimental results are checked for water and nanofluids at a given flow rate, and it is observed that Reynolds number decreases with concentration. But, the decrease rate due to viscosity is much lower than the decrease in the onsets. Hence, nanoparticle addition is more solid explanation regarding early transition.

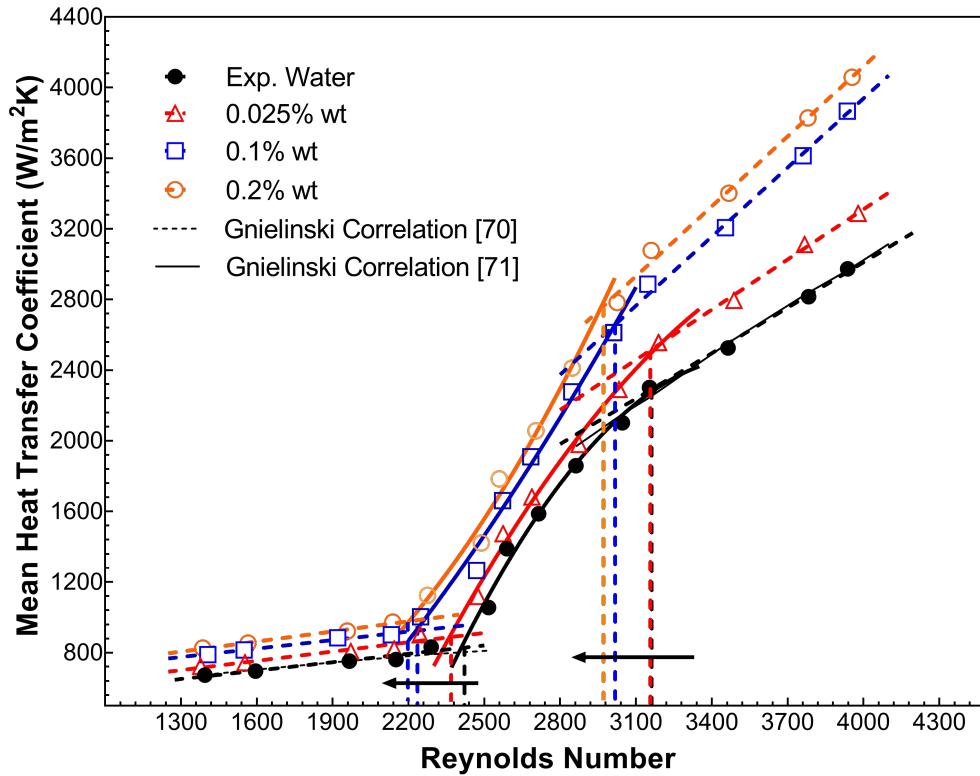


Figure 3.19. Mean heat transfer coefficient change trends of graphene-water nanofluids with 0.025, 0.1 and 0.2% mass concentration for laminar, transition and turbulent flow

The effect of thermal conduction begins to diminish after transition regime. In Figure 3.20, the Nusselt numbers of the nanofluids are very close to each other due to the heat conduction, whereas the increase in mean Nusselt number starts to be observed as the convection mechanism increases the heat transfer significantly in higher Reynolds number. The mean heat transfer coefficient enhancement for the nanofluid with 0.025% concentration becomes more pronounced beyond a Reynolds number of 3100 and maximum enhancement is 11% at $Re_D=3200$. Also, the nanofluids with 0.1 and 0.2% particle mass fractions reach the early turbulent state around $Re_D=3000$. The maximum augmentation in the mean heat transfer coefficient is 30% and 36% for the nanofluids with 0.1 and 0.2% fraction at a Reynolds number of 3950, respectively. The results are in agreement with the literature [53, 56]. Thermal conduction might have the key role for explaining the heat transfer mechanisms in here. It is stated

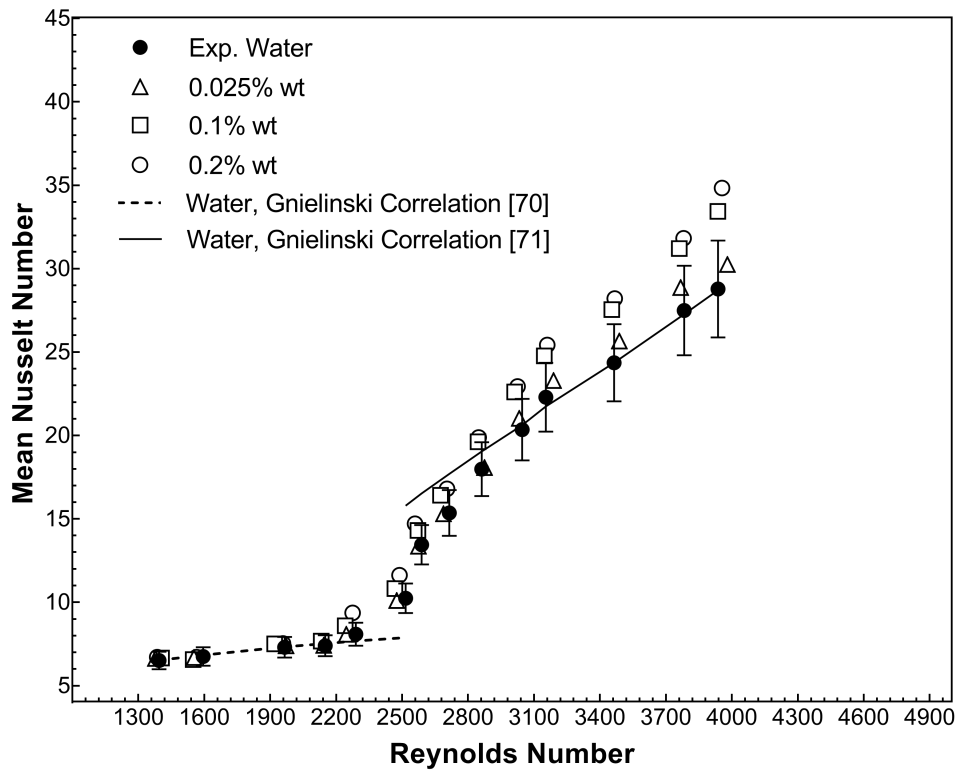


Figure 3.20. Mean Nusselt number change of graphene-water nanofluids for 0.025, 0.1 and 0.2% mass concentration

before, graphene nanoparticles create percolation chains in the nanofluids and increase the thermal conductivity. In the steady-state laminar flow conditions, percolation chains might keep their formations and create local zones where thermal conduction dominates the heat transfer enhancement. Beyond laminar region, the instabilities and random fluctuations in the flow break the percolation chains and decrease the conduction effect. Eventually, convective mechanisms such as thermophoresis leads to enhance the heat transfer rather than thermal conduction in the turbulent flow [89], and heat transfer increases much more than laminar flow.

In order to investigate the heating effects on the structure of the graphene-water nanofluids, viscosity of the nanofluids is measured before and after the experiments. The measurements are performed in the temperature range of 25 to 50 °C, repeated three times, and the average values are calculated. The maximum change in the relative

viscosity before and after the tests is seen as less than $\pm 2\%$. Hence, the structure of prepared nanofluids are not affected from heating process significantly.

4. CONCLUSION AND FUTURE WORK

4.1. Conclusion

A preparation recipe for graphene-water nanofluids is developed and thermo-physical properties of produced nanofluids are investigated for a particle mass fraction range of 0.025-2%. The nanofluids are prepared using two-step method, using mechanical and ultrasonic mixing, and PVP with surfactant-nanoparticle mass ratio of 1-1 to achieve stable suspensions. Particle size and aggregation level of the purchased dry graphene nano-flakes are characterized by ESEM images, and Raman spectroscopy is used to identify the graphene nano-flakes. Temporal zeta potential measurements are also performed for determining the stability level over a period of 30 days and DLS measurements are used to identify the mean particle size. Moreover, STEM imaging is used for dried nanofluids for morphological investigation. The rheological behavior is measured using cone-plate rheometer at different temperatures and shear rates, and thermal conductivity is measured using transient hot wire thermal analyzer.

It is observed that the nanofluids produced with the developed recipe are stable up to 30 days based on Zeta potential measurements. Dynamic viscosity of the prepared nanofluids is measured in the range of 0.1-2% particle mass fraction. The maximum viscosity increase with respect to base fluid is 45% for 2% concentration and amount of the increase in viscosity ascends after 1%. Moreover, the produced graphene-water nanofluids exhibit Newtonian behavior for lower particle mass fractions ($<1\%$) and shear thinning behavior is observed for higher particle concentrations ($\geq 1\%$). Besides, the shear thinning behavior is more pronounced for higher temperatures. It was identified that the shear thinning behavior is due to disintegration of the percolating structures that are observed in STEM images. A hysteresis behavior is also observed for viscosity; nanofluids with relatively higher particle concentration and at higher temperatures exhibit more pronounced shear thinning behavior for experiments with decreasing shear rates, rather than increasing. Significant increase in

thermal conductivity with respect to that of base fluid is observed for the produced nanofluids. The nanofluid with 0.1% and 2% particle mass fraction exhibits 22%, and 98% increase in thermal conductivity, with respect to that of the base fluid.

Forced convection in graphene-water nanofluids is investigated for 0.025, 0.1 and 0.2% particle mass concentrations. Experiments are carried out for a Reynolds number range of 1400 to 4000 by focusing on the transition flow regime. Pressure drop and friction factor change are measured by two pressure transducers that are placed to the inlet and outlet of the test pipe. Studied nanofluids show similar friction factor increase trend in the transition region. Also, pressure drop increase in the studied nanofluids do not exceed 10% with respect to the water in the laminar and turbulent flow, but it increases up to the 30% within transition regime. The convective heat transfer performance of the graphene-water nanofluids is also investigated. The study is done at laminar, transition and turbulent regions in order to understand the effective mechanisms on the convective heat transfer. In laminar region, local heat transfer coefficient enhancement for given nanofluids at $x/D=120$ and $x/D=240$ roughly does not change with Reynolds number. Besides, thermal conduction enhancement mechanisms dominates the heat transfer enhancement and all nanofluids have similar Nusselt number for given Reynolds numbers and axial locations, whereas increase in the mean heat transfer coefficient is about 7, 17 and 22%. Then, it is observed that transition from laminar flow for the graphene-water nanofluids in the concentration range studied shifts to the lower Reynolds numbers. The transition relying on the heat transfer measurements begins at lower Reynolds numbers than measurements relying on the friction factor. It means that increase in the mean heat transfer coefficient for nanofluids starts just before the transition flow. By relying on the heat transfer measurements, the mean heat transfer coefficients of the nanofluids with 0.025%, 0.1% and 0.2% particle mass concentrations increase significantly after at a Reynolds number of 2370, 2250 and 2200, respectively, whereas it is about 2450 for DI water. For the nanofluids of 0.1 and 0.2% concentrations, the enhancement in the mean heat transfer coefficient is observed

after around a Reynolds number of 3000. Furthermore, prepared nanofluids exhibit maximum 36% mean heat transfer coefficient enhancement for 0.2% particle mass concentration at a Reynolds number of 3950.

In conclusion, graphene-water nanofluids provide an outstanding heat transfer enhancement by creating percolation structures. Hysteresis phenomenon is observed in high concentrations and temperatures. Also, pressure drop increase is relatively low in the laminar and turbulent regime, whereas it is higher in the transition flow. Therefore, it should not be preferred to work with graphene-water nanofluids in the transition region as it causes the relatively high pressure drop and pumping power.

4.2. Recommendations for Future Work

Considering the observed stability, significant increase in thermal conductivity that exceeds the viscosity increase; graphene-water nanofluids have a significant potential for thermal management or energy system applications. Further experimental studies should be carried out to identify the effective heat transfer mechanisms beyond laminar flow regime, and microscopic modeling must be utilized to further validate the hypothesis outlined explaining the hysteresis observed and the shear thinning behavior. Also, applications such as direct absorption solar systems, electronics and vehicle thermal management might be deeply investigated by using the graphene-water nanofluids.

REFERENCES

1. Das, S. K., S. U. S. Choi and H. E. Patel, “Heat Transfer in Nanofluids - A Review”, *Heat Transfer Engineering*, Vol. 27, No. 10, pp. 3–19, 2006.
2. Choi, S. U. S., “Enhancing Thermal Conductivity of Fluids with Nanoparticles”, *American Society of Mechanical Engineers Fluids Engineering Division, FED*, 1995.
3. Baby, T. T. and S. Ramaprabhu, “Investigation of Thermal and Electrical Conductivity of Graphene Based Nanofluids”, *Journal of Applied Physics*, Vol. 108, 2010.
4. Sezer, N., M. A. Atieh and M. Koç, “A Comprehensive Review on Synthesis Stability, Thermophysical Properties, and Characterization of Nanofluids”, *Powder Technology*, Vol. 344, pp. 404–431, 2019.
5. Yu, W. and H. Xie, “A Review on Nanofluids: Preparation, Stability Mechanisms, and Applications”, *Journal of Nanomaterials*, Vol. 2012, 2012.
6. Rasheed, A. K., M. Khalid, W. Rashmi, T. C. S. M. Gupta and A. Chan, “Graphene Based Nanofluids and Nanolubricants - Review of Recent Developments”, *Renewable and Sustainable Energy Reviews*, Vol. 63, pp. 346–362, 2016.
7. Ilhan, B., M. Kurt and H. Ertürk, “Experimental Investigation of Heat Transfer Enhancement and Viscosity Change of hBN Nanofluids”, *Experimental Thermal and Fluid Science*, Vol. 77, pp. 272–283, 2016.
8. Borode, A. O., N. A. Ahmed and P. A. Olubambi, “Surfactant-aided Dispersion of Carbon Nanomaterials in Aqueous Solution,”, *Physics of Fluids*, Vol. 31, 2019.
9. Sadeghinezhad, E., M. M. Mehrali, R. Saidur, M. M. Mehrali, S. T. Latibari,

- A. R. Akhiani and H. S. C. Metselaar, “A Comprehensive Review on Graphene Nanofluids: Recent Research, Development and Applications”, *Energy Conversion and Management*, Vol. 111, pp. 466–487, 2016.
10. Yu, F., Y. Chen, X. Liang, J. Xu, C. Lee, Q. Liang, P. Tao and T. Deng, “Dispersion Stability of Thermal Nanofluids”, *Progress in Natural Science: Materials International*, Vol. 27, pp. 531–542, 2017.
 11. Keblinski, P., R. Phillpot, S. Choi and A. Eastman, “Mechanisms of Heat Flow in Suspensions of Nano-sized Particles (Nanofluids)”, *International Journal of Heat and Mass Transfer*, Vol. 45, pp. 855–863, 2002.
 12. Jang, S. P. and S. U. S. Choi, “Role of Brownian Motion in the Enhanced Thermal Conductivity of Nanofluids”, *Applied Physics Letters*, Vol. 84, pp. 4316–4318, 2004.
 13. Kumar, D. H., H. E. Patel, V. R. R. Kumar, T. Sundararajan, T. Pradeep and S. K. Das, “Model for Heat Conduction in Nanofluids”, *Physical Review Letters*, Vol. 93, pp. 1–4, 2004.
 14. Xie, H., M. Fujii and X. Zhang, “Effect of Interfacial Nanolayer on the Effective Thermal Conductivity of Nanoparticle-fluid Mixture”, *International Journal of Heat and Mass Transfer*, Vol. 48, pp. 2926–2932, 2005.
 15. Gao, J. W., R. T. Zheng, H. Ohtani, D. S. Zhu and G. Chen, “Experimental Investigation of Heat Conduction Mechanisms in Nanofluids. Clue on Clustering”, *Nano Letters*, Vol. 9, pp. 4128–4132, 2009.
 16. Chandrasekar, M. and S. Suresh, “A Review on the Mechanisms of Heat Transport in Nanofluids”, *Heat Transfer Engineering*, Vol. 30, pp. 1136–1150, 2009.
 17. Chon, C. H., K. D. Kihm and U. S. Choi, “Empirical Correlation Finding the Role of Temperature and Particle Size for Nanofluid (Al₂O₃) Thermal Conductivity Enhancement”, *Applied Physics Letters*, Vol. 153107, pp. 1–4, 2005.

18. Das, S. K., N. Putra, P. Thiesen and W. Roetzel, "Temperature Dependence of Thermal Conductivity Enhancement for Nanofluids", *Journal of Heat Transfer*, Vol. 125, pp. 567–574, 2003.
19. Duangthongsuk, W. and S. Wongwises, "Measurement of Temperature-dependent Thermal Conductivity and Viscosity of TiO₂-Water Nanofluids", *Experimental Thermal and Fluid Science*, Vol. 33, pp. 706–714, 2009.
20. Jeong, J., C. Li, Y. Kwon, J. Lee, S. Hyung and R. Yun, "Particle Shape Effect on the Viscosity and Thermal Conductivity of ZnO Nanofluids", *International Journal of Refrigeration*, Vol. 36, pp. 2233–2241, 2013.
21. Ding, Y., H. Alias, D. Wen and R. A. Williams, "Heat Transfer of Aqueous Suspensions of Carbon Nanotubes (CNT Nanofluids)", *International Journal of Heat and Mass Transfer*, Vol. 49, pp. 240–250, 2006.
22. Abareshi, M., E. K. Goharshadi, S. M. Zebarjad, H. K. Fadafan and A. Youssefi, "Fabrication, Characterization and Measurement of Thermal Conductivity of Fe₃O₄ Nanofluids", *Journal of Magnetism and Magnetic Materials*, 2010.
23. Vajjha, R. S. and D. K. Das, "A Review and Analysis on Influence of Temperature and Concentration of Nanofluids on Thermophysical Properties, Heat Transfer and Pumping Power", *International Journal of Heat and Mass Transfer*, Vol. 55, pp. 4063–4078, 2012.
24. Chandrasekar, M., S. Suresh and A. C. Bose, "Experimental Investigations and Theoretical Determination of Thermal Conductivity and Viscosity of Al₂O₃/water Nanofluid", *Experimental Thermal and Fluid Science*, Vol. 34, pp. 210–216, 2010.
25. Nguyen, C. T., F. Desgranges, G. Roy, N. Galanis, T. Maré, S. Boucher and H. A. Mintsa, "Temperature and Particle-size Dependent Viscosity Data for Water-based Nanofluids - Hysteresis Phenomenon", *International Journal of Heat and Mass*

- Transfer*, Vol. 28, pp. 1492–1506, 2007.
26. Phuoc, T. X., M. Massoudi and R. H. Chen, “Viscosity and Thermal Conductivity of Nanofluids Containing Multi-walled Carbon Nanotubes Stabilized by Chitosan”, *International Journal of Thermal Sciences*, Vol. 50, pp. 12–18, 2011.
 27. Nguyen, C. T., F. Desgranges, G. Roy, N. Galanis, T. Maré, S. Boucher and H. A. Mintsa, “Viscosity Data for Al₂O₃-water Nanofluid-Hysteresis: Is Heat Transfer Enhancement Using Nanofluids Reliable?”, *International Journal of Thermal Science*, Vol. 47, pp. 103–111, 2008.
 28. Jiang, W., K. Du, Y. Li and L. Yang, “Étude Expérimentale Sur L’Influence De La Température Élevée Sur La Viscosité, La Conductivité Thermique Et L’Absorbance Des Nanofluides Ammoniac-Eau”, *International Journal of Refrigeration*, Vol. 82, pp. 189–198, 2017.
 29. Aladag, B., S. Halelfadl, N. Doner, T. Maré, S. Duret and P. Estellé, “Experimental Investigations of the Viscosity of Nanofluids at Low Temperatures”, *Applied Energy*, Vol. 97, p. 876–880, 2012.
 30. Wang, J. J., R. T. Zheng, J. W. Gao and G. Chen, “Heat Conduction Mechanisms in Nanofluids and Suspensions”, *Nano Today*, Vol. 7, pp. 124–136, 2012.
 31. Liu, M. S., M. C.-C. Lin, I. T. Huang and C. C. Wang, “Enhancement of Thermal Conductivity with Carbon Nanotube for Nanofluids”, *International Communications in Heat and Mass Transfer*, Vol. 32, No. 9, pp. 1202–1210, 2005.
 32. Novoselov, K. S., “Electric Field Effect in Atomically Thin Carbon Films”, *Science*, Vol. 80, pp. 666–669, 2004.
 33. Kole, M. and T. K. Dey, “Investigation of Thermal Conductivity, Viscosity, and Electrical Conductivity of Graphene Based Nanofluids”, *Journal of Applied Physics*, Vol. 113, 2013.

34. Balandin, A. A., S. Ghosh, W. Bao, I. Calizo, D. Teweldebrhan, F. Miao and C. N. Lau, “Superior Thermal Conductivity of Single-Layer Graphene”, *Nano Letters*, Vol. 8, pp. 902–907, 2008.
35. Geim, A. K. and K. S. Novoselov, “The Rise of Graphene”, *Nature Materials*, Vol. 6, pp. 183–191, 2007.
36. Yu, W., H. Xie and D. Bao, “Enhanced Thermal Conductivities of Nanofluids Containing Graphene Oxide Nanosheets”, *Nanotechnology.*, Vol. 21, p. 055705, 2010.
37. Yu, W., H. Xie, X. Wang and X. Wang, “Significant Thermal Conductivity Enhancement for Nanofluids Containing Graphene Nanosheets”, *Physics Letters Section A*, Vol. 375, pp. 1323–1328, 2011.
38. Gupta, S. S., M. V. Siva, S. Krishnan, T. S. Sreeprasad, P. K. Singh, T. Pradeep, S. K. Das, S. S. Gupta, V. M. Siva, S. Krishnan, T. S. Sreeprasad, P. K. Singh, T. Pradeep and S. K. Das, “Thermal Conductivity Enhancement of Nanofluids Containing Graphene Nanosheets”, *Journal of Applied Physics*, Vol. 110, p. 084302, 2011.
39. Mehrali, M., E. Sadeghinezhad, S. T. Latibari, S. N. Kazi, M. Mehrali, M. Nashrul, B. Mohd, H. Simon and C. Metselaar, “Investigation of Thermal Conductivity and Rheological Properties of Nanofluids Containing Graphene Nanoplatelets”, *Nanoscale Research Letters*, pp. 1–12, 2014.
40. Hajjar, Z., A. M. Rashidi and A. Ghozatloo, “Enhanced Thermal Conductivities of Graphene Oxide Nanofluids”, *International Communications Heat and Mass Transfer*, Vol. 57, pp. 128–131, 2014.
41. Ghozatloo, A., M. Shariaty-Niasar and A. M. Rashidi, “Preparation of Nanofluids From Functionalized Graphene by New Alkaline Method and Study on the Ther-

- mal Conductivity and Stability”, *International Communications in Heat and Mass Transfer*, Vol. 42, pp. 89–94, 2013.
42. Moghaddam, M. B., E. K. Goharshadi, M. H. Entezari and P. Nancarrow, “Preparation, Characterization, and Rheological Properties of Graphene-glycerol Nanofluids”, *Chemical Engineering Journal*, 2013.
43. Sarsam, W. S., A. Amiri, S. N. Kazi and A. Badarudin, “Stability and Thermophysical Properties of Non-covalently Functionalized Graphene Nanoplatelets Nanofluids”, *Energy Conversion and Management*, Vol. 116, pp. 101–111, 2016.
44. Yang, L., W. Ji, Z. Zhang and X. Jin, “Thermal Conductivity Enhancement of Water by Adding Graphene Nano-sheets: Consideration of Particle Loading and Temperature Effects”, *International Communications in Heat and Mass Transfer*, Vol. 109, No. 10435, p. 3, 2019.
45. Heyhat, M. M., F. Kowsary, A. M. Rashidi, M. H. Momenpour and A. Amrollahi, “Experimental Investigation of Laminar Convective Heat Transfer and Pressure Drop of Water-Based Al₂O₃ Nanofluids in Fully Developed Flow Regime”, *Experimental Thermal and Fluid Science*, Vol. 44, pp. 483–489, 2013.
46. Pak, B. C. and Y. I. Cho, “Hydrodynamic and Heat Transfer Study of Dispersed Fluids with Submicron Metallic Oxide Particles”, *Experimental Heat Transf.*, Vol. 11, pp. 151–170, 1998.
47. Heris, S. Z., S. G. Etemad, M. N. Esfahany and S. Z. Heris, “Convective Heat Transfer of a Cu/Water Nanofluid Flowing Through a Circular Tube”, *Experimental Heat Transfer*, Vol. 22, pp. 217–227, 2009.
48. Fotukian, S. M. and M. N. Esfahany, “Experimental Study of Turbulent Convective Heat Transfer and Pressure Drop of Dilute CuO/water Nanofluid Inside a Circular Tube”, *International Communications in Heat and Mass Transfer*, Vol. 37, pp.

- 214–219, 2010.
49. Kayhani, M. H., H. Soltanzadeh, M. M. Heyhat, M. Nazari and F. Kowsary, “Experimental Study of Convective Heat Transfer and Pressure Drop of TiO₂/Water Nanofluid”, *International Communications in Heat and Mass Transfer*, Vol. 39, pp. 456–462, 2012.
 50. Esfe, M. H., S. Saedodin, M. Biglari and H. Rostamian, “An Experimental Study on Thermophysical Properties and Heat Transfer Characteristics of Low Volume Concentrations of Ag-water Nanofluid”, *International Communications in Heat and Mass Transfer*, Vol. 74, pp. 91–97, 2016.
 51. Wang, J., J. Zhu, X. Zhang and Y. Chen, “Heat Transfer and Pressure drop of Nanofluids Containing Carbon Nanotubes in Laminar Flows”, *Experimental Thermal and Fluid Science*, Vol. 44, pp. 716–721, 2013.
 52. Baby, T. and S. Ramaprabhu, “Enhanced Convective Heat Transfer Using Graphene Dispersed Nanofluids”, *Nanoscale Research Letters*, Vol. 6, p. 289, 2011.
 53. Ghozatloo, A., A. Rashidi and M. Shariaty-Niassar, “Convective Heat Transfer Enhancement of Graphene Nanofluids in Shell and Tube Heat Exchanger”, *Experimental Thermal and Fluid Science*, Vol. 53, pp. 136–141, 2014.
 54. Akhavan-Zanjani, H., M. Saffar-Avval, M. Mansourkiaei, F. Sharif and M. Ahadi, “Experimental Investigation of Laminar Forced Convective Heat Transfer of Graphene-water Nanofluid Inside a Circular Tube”, *International Journal of Thermal Sciences*, Vol. 100, pp. 316–323, 2016.
 55. Selvam, C., T. Balaji, D. M. Lal and S. Harish, “Convective Heat Transfer Coefficient and Pressure Drop of Water-Ethylene Glycol Mixture with Graphene Nanoplatelets”, *Experimental Thermal and Fluid Science*, Vol. 80, pp. 67–76, 2017.
 56. Yarmand, H., S. Gharekhani, S. F. S. Shirazi, A. Amiri, M. S. Alehashem,

- M. Dahari and S. N. Kazi, “Experimental Investigation of Thermo-physical Properties, Convective Heat Transfer and Pressure Drop of Functionalized Graphene Nanoplatelets Aqueous Nanofluid in a Square Heated Pipe”, *Energy Conversion and Management*, Vol. 114, pp. 38–49, 2016.
57. Arshad, A., M. Jabbal, Y. Yan and D. Reay, “A review on graphene based nanofluids: Preparation, characterization and applications”, *Journal of Molecular Liquids journal*, pp. 444–484, 2019.
58. Bahiraei, M. and S. Heshmatian, “Graphene Family NanoFluids: A Critical Review and Future Research Directions”, *Energy Conversion and Management*, Vol. 196, pp. 1222–1256, 2019.
59. Wang, T., M. D. J. Quinn and S. M. Notley, “Enhanced Electrical, Mechanical and Thermal Properties by Exfoliating Graphene Platelets of Larger Lateral Dimensions”, *Carbon*, Vol. 129, pp. 191–198, 2018.
60. Yoon, S. and I. In, “Role of poly(N-vinyl-2-pyrrolidone) as Stabilizer for Dispersion of Graphene via Hydrophobic Interaction”, *Journal of Materials Science*, Vol. 46, pp. 1316–1321, 2011.
61. Zhao, S., G. Xu, N. Wang and X. Zhang, “Experimental Study on the Thermal Start-up Performance of the Graphene/water Nanofluid-enhanced Solar Gravity Heat Pipe”, *Nanomaterials*, Vol. 8, 2018.
62. Ilhan, B. and H. Erturk, “Experimental Characterization of Laminar Forced Convection of hBN-water Nanofluid in Circular Pipe”, *International Journal of Heat and Mass Transfer*, Vol. 111, pp. 500–507, 2017.
63. Lotya, M., A. Rakovich, J. F. Donegan and J. N. Coleman, “Measuring the Lateral Size of Liquid-exfoliated Nanosheets with Dynamic Light Scattering”, *Nanotechnology*, Vol. 24, 2013.

64. Wang, J., F. Ma and M. Sun, “Graphene, Hexagonal Boron Nitride, and Their Heterostructures: Properties and Applications”, *Royal Society of Chemistry Advances*, Vol. 7, pp. 16801–16822, 2017.
65. Fan, D., Q. Li, W. Chen and J. Zeng, “Graphene Nanofluids Containing Core-shell Nanoparticles With Plasmon Resonance Effect Enhanced Solar Energy Absorption”, *Solar Energy*, Vol. 158, pp. 1–8, 2017.
66. Selvam, C., D. M. Lal and S. Harish, “Thermal Conductivity and Specific Heat Capacity of Water-Ethylene Glycol Mixture-based Nanofluids with Graphene Nanoplatelets”, *Journal of Thermal Analysis and Calorimetry*, Vol. 129, pp. 947–955, 2017.
67. D7896-19, A., “Standard Test Method for Thermal Conductivity Thermal Diffusivity and Volumetric Heat Capacity of Engine Coolants and Related Fluids by Transient Hot Wire Liquid Thermal Conductivity Method”, , 2014.
68. Petukhov, B. S., “Heat Transfer and Friction in Turbulent Pipe Flow with Variable Physical Properties”, *Advances in Heat Transfer*, 1970.
69. Shah, R. K. and A. L. London, *Laminar Flow Forced Convection in Ducts: A Source article for Compact Heat Exchanger Analytical Data*, Vol. 1978, Academic Press, 1978.
70. Gnielinski, V., “On Heat Transfer in Tubes”, *International Journal of Heat and Mass Transfer*, Vol. 63, pp. 134–140, 2013.
71. Gnielinski, V., “New Equations for Heat and Mass Transfer in Turbulent Pipe and Channel Flow”, *International Chemical Engineering*, 1976.
72. Kline, S. and F. McClintock, “Describing Uncertainties in Single-sample Experiments”, *Mechanical Engineering*, 1953.

73. Esfahani, M. R., E. M. Languri and M. R. Nunna, “Effect of Particle Size and Viscosity on Thermal Conductivity Enhancement of Graphene Oxide Nanofluid”, *International Communications in Heat and Mass Transfer*, Vol. 76, pp. 308–315, 2016.
74. Li, P., Y. Zheng, Y. Wu, P. Qu, R. Yang and A. Zhang, “Nanoscale Ionic Graphene Material with Liquid-like Behavior in the Absence of Solvent”, *Applied Surface Science*, Vol. 314, pp. 983–990, 2014.
75. Prasher, R., P. Bhattacharya and P. E. Phelan, “Brownian Motion-based Convective Conductive Model for the Effective Thermal Conductivity of Nanofluids”, *Journal of Heat Transfer*, Vol. 128, p. 588, 2006.
76. Wang, B., J. Hao and H. Li, “Remarkable Improvements in the Stability and Thermal Conductivity of Graphite/ethylene glycol Nanofluids Caused by a Graphene Oxide Percolation Structure”, *Dalton Transactions*, Vol. 42, p. 5866, 2013.
77. Batchelor, G. K., “The Effect of Brownian Motion on the Bulk Stress in a Suspension of Spherical Particles”, *Journal of Fluid Mechanics*, 1977.
78. Selvam, C., D. M. Lal and S. Harish, “Thermal Conductivity Enhancement of Ethylene Glycol and Water with Graphene Nanoplatelets”, *Thermochimica Acta*, Vol. 642, pp. 32–38, 2016.
79. Mehrali, M., E. Sadeghinezhad, S. T. Latibari, M. Mehrali, H. Togun, M. N. M. Zubir, S. N. Kazi and H. S. C. Metselaar, “Preparation, Characterization, Viscosity, and Thermal Conductivity of Nitrogen-doped Graphene Aqueous Nanofluids”, *Journal of Material Science*, Vol. 49, pp. 7156–7171, 2014.
80. Ahammed, N., L. G. Asirvatham and S. Wongwises, “Effect of Volume Concentration and Temperature on Viscosity and Surface Tension of Graphene-water Nanofluid for Heat Transfer Applications”, *Journal of Thermal Analysis and*

Calorimetry, Vol. 123, pp. 1399–1409, 2015.

81. Shazali, S., A. Amiri, M. Nashrul, M. Zubir, S. Rozali, M. Zakuan, M. Faizul and M. Sabri, “Investigation of the Thermophysical Properties and Stability Performance of Non-covalently Functionalized Graphene Nanoplatelets with Pluronic P-123 in different solvents”, *Materials Chemistry and Physics*, Vol. 206, pp. 94–102, 2018.
82. Naddaf, A. and S. Z. Heris, “Experimental Study on Thermal Conductivity and Electrical Conductivity of Diesel Oil-based Nanofluids of Graphene Nanoplatelets and Carbon Nanotubes”, *International Communications in Heat and Mass Transfer*, pp. 116–122, 2018.
83. Rudyak, V. Y., A. V. Minakov, D. V. Guzey, V. A. Zhigarev and M. I. Pryazhnikov, “On Laminar-Turbulent Transition in Nanofluid Flows”, *Thermophysics and Aeromechanics*, Vol. 23, pp. 773–776, 2016.
84. Meyer, J. P., T. J. McKrell and K. Grote, “The Influence of Multi-walled Carbon Nanotubes on Single-phase Heat Transfer and Pressure Drop Characteristics in The Transitional Flow Regime of Smooth Tubes”, *International Journal of Heat and Mass Transfer*, Vol. 58, pp. 597–609, 2013.
85. Nikulin, A., A. S. Moita, A. L. N. Moreira, S. M. S. Murshed, A. Huminic, Y. Grosu, A. Faik, J. Nieto-Maestre and O. Khliyeva, “Effect of Al₂O₃ Nanoparticles on Laminar, Transient and Turbulent Flow of Isopropyl Alcohol”, *International Journal of Heat and Mass Transfer*, Vol. 130, pp. 1032–1044, 2019.
86. Sommers, A. D., K. L. Yerkes and A. R. Runyon, “A Study of the Thermal-Hydraulic Performance and System-Level Effects of Aluminum Oxide-Propanol Nanofluid”, *Proceedings of the 2010 14th International Heat Transfer Conference*, Vol. 6, pp. 631–639, 2011.

87. Singh, P. K., T. Sundararajan and S. K. Das, “Hydrodynamic Study of Nanofluids in Microchannel”, *ASME Second International Conference on Micro/Nanoscale Heat and Mass Transfer*, pp. 467–473, 2010.
88. Tang, C. C., S. Tiwari and M. W. Cox, “Viscosity and Friction Factor of Aluminum Oxide-Water Nanofluid Flow in Circular Tubes”, *Journal of Nanotechnology*, 2013.
89. Saxena, R., D. Gangacharyulu and V. K. Bulasara, “Heat Transfer and Pressure Drop Characteristics of Dilute Alumina–Water Nanofluids in a Pipe at Different Power Inputs”, *Heat Transfer Engineering*, Vol. 37, pp. 1554–1565, 2016.

APPENDIX A: ESEM IMAGES OF DRY GRAPHENE NANOPARTICLES

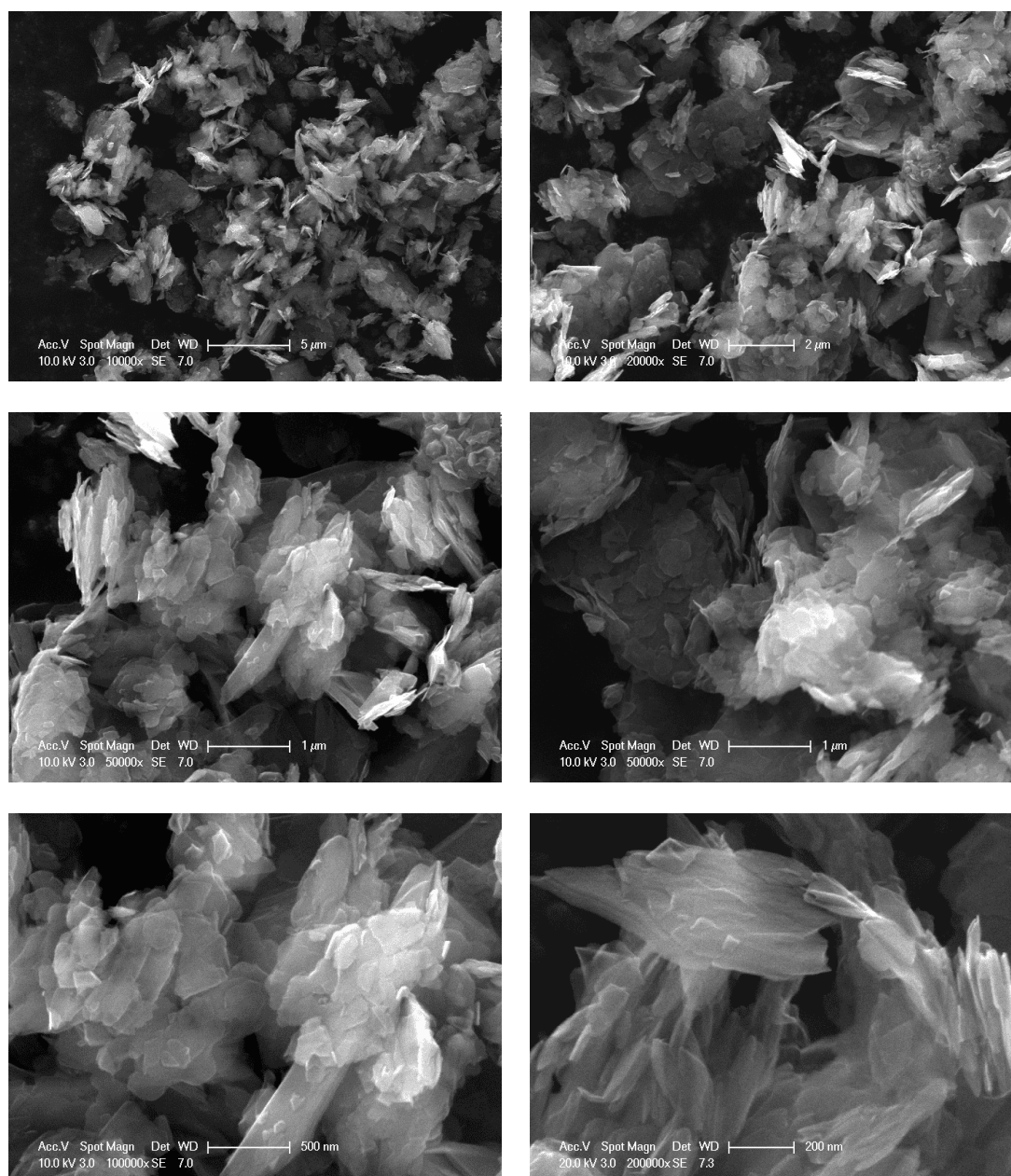


Figure A.1. ESEM images of dry graphene nanoparticles in different scales

APPENDIX B: STEM IMAGES OF GRAPHENE-WATER NANOFLUIDS

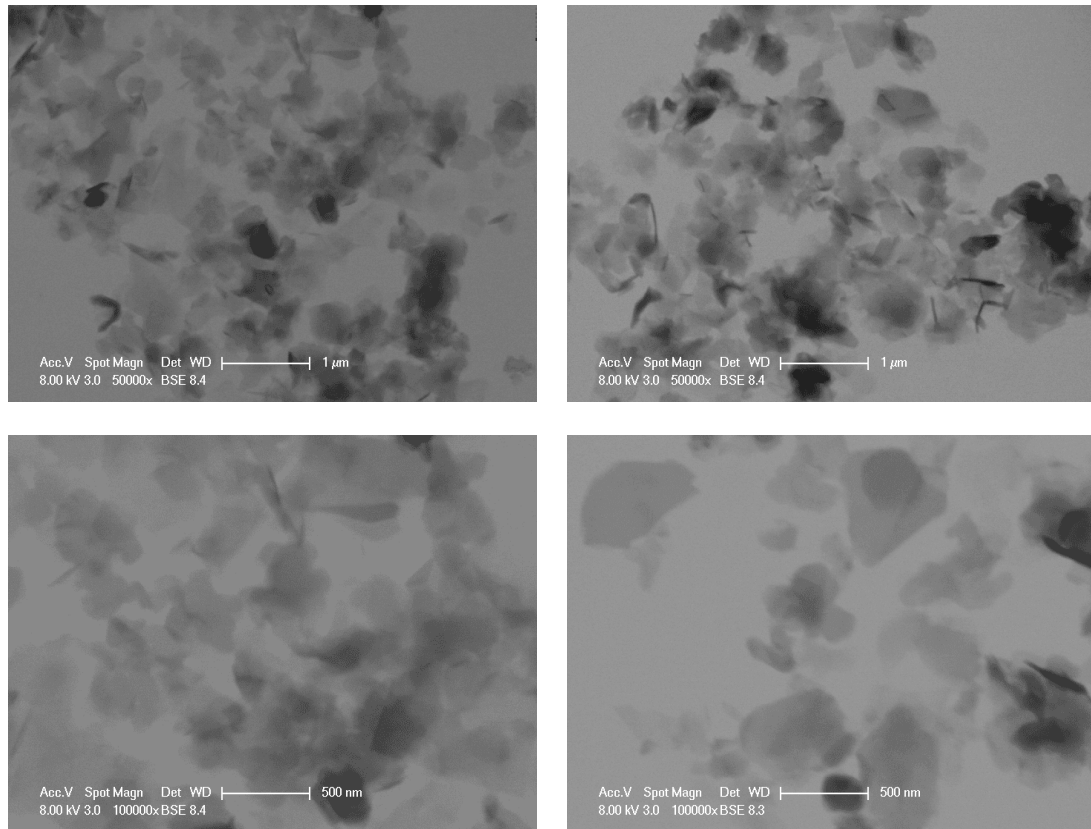


Figure B.1. STEM images of graphene-water nanofluids with the particle mass concentration of 0.1% in different scales

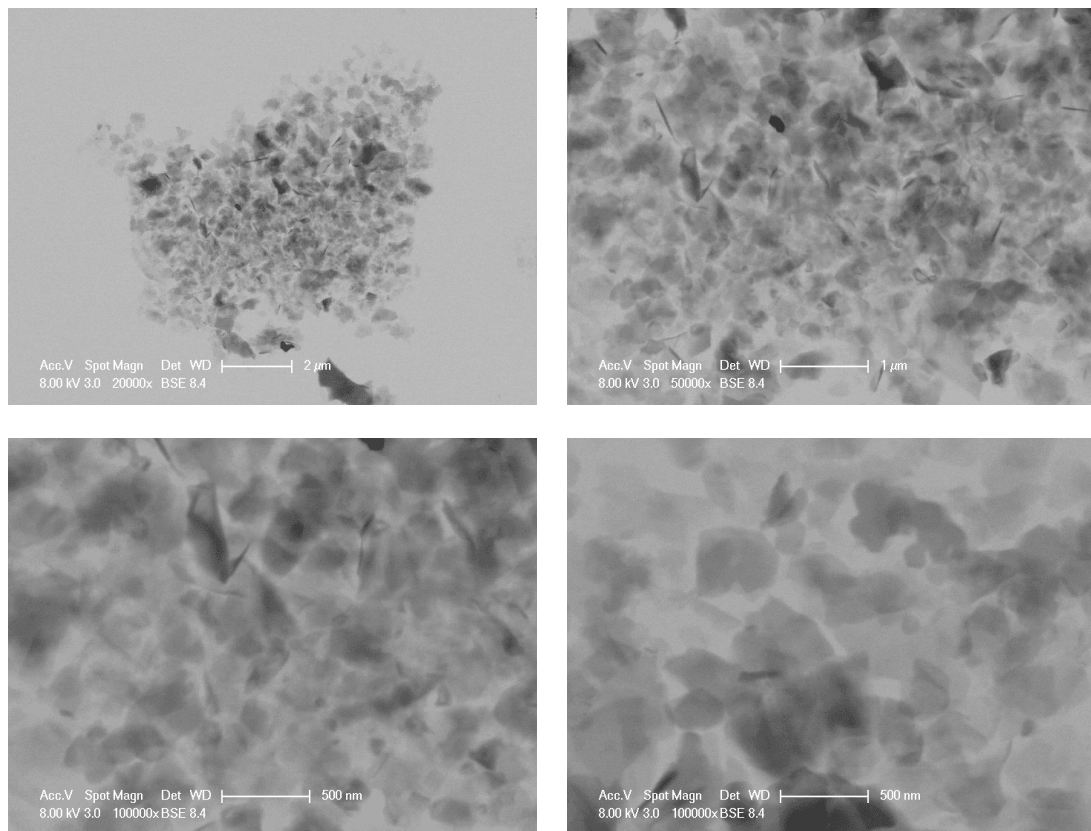


Figure B.2. STEM images of graphene-water nanofluids with the particle mass concentration of 0.5% in different scales

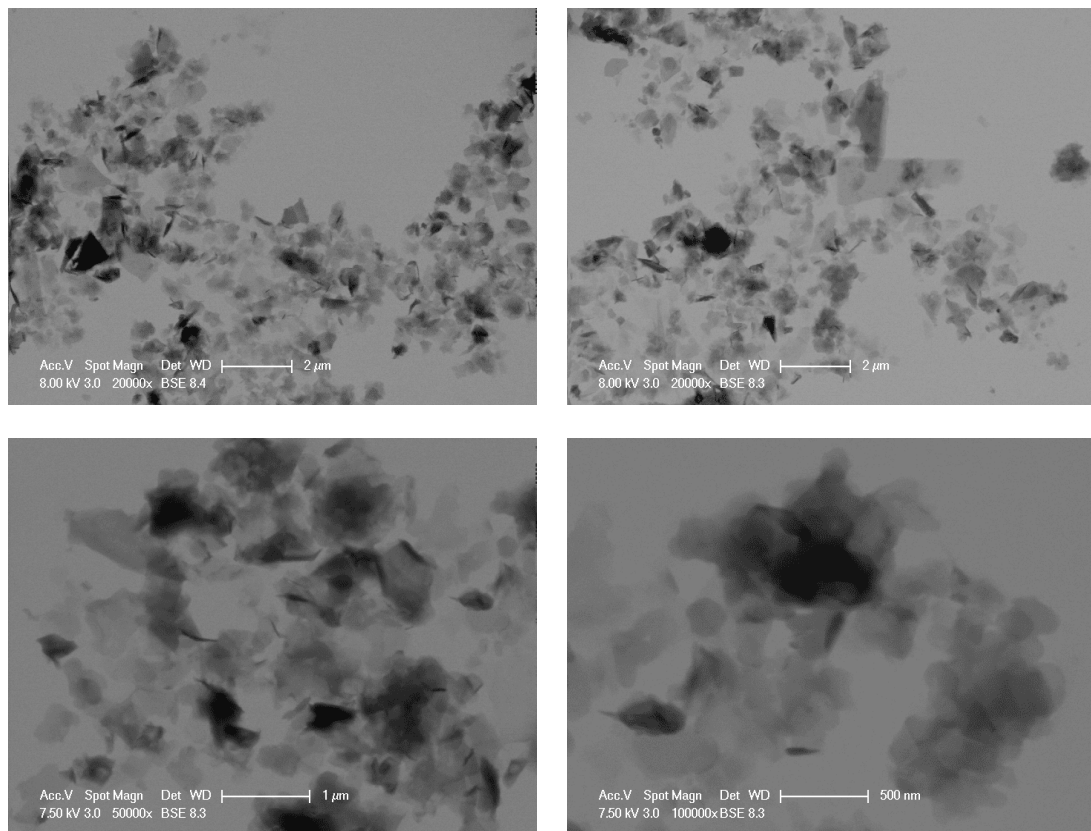


Figure B.3. STEM images of graphene-water nanofluids with the particle mass concentration of 1% in different scales

APPENDIX C: CONVECTIVE HEAT TRANSFER DATA SET FOR WATER AT A REYNOLDS NUMBER OF 1400

The values used in the convective heat transfer calculations for DI water at a Reynolds number of 1400 are listed in Table C.1. Local heat transfer coefficients and local Nusselt numbers calculated from the values in Table C are shown in Table C.2.

Table C.1. The parameters used in the heat transfer calculations for water
at $Re_D=1400$

Parameter	Value	Unit
Pipe Inside Diameter	0.006	m
Density	993.56	kg/m ³
Dynamic Viscosity	0.0007	kg/m.s
Specific Heat	4180	J/kg.K
Thermal Conductivity	0.625	W/m.K
Volume Flow Rate	4.64E-06	m ³ /s
Mass Flow Rate	0.00461	kg/s
Inlet Flow Temperature	26.59	°C
Outlet Flow Temperature	46.12	°C
Power Supplied to Heater	400	W
Heat Transferred to System	376.11	W
Heat Flux	13302.2	W/m ²

Table C.2. Measured wall and inlet temperatures, and local heat transfer coefficients along the test pipe for DI water at $Re_D=1400$

x/D_h	T_x (°C)	$T_{m,i}$ (°C)	$T_m(x)$ (°C)	Experimental h_x	Experimental Nu_x
10	39.18	26.59	27.37	1126.67	10.82
33.33	46.70	26.59	29.20	759.73	7.29
46.66	48.80	26.59	30.24	716.58	6.88
60	51.22	26.59	31.28	667.16	6.4
80	55.06	26.59	32.84	598.84	5.75
100	57.54	26.59	34.41	574.99	5.52
120	60.38	26.59	35.97	544.97	5.23
200	67.86	26.59	42.22	518.79	4.98
240	71.80	26.59	45.35	502.84	4.83